**The *Arabidopsis* 14-3-3 proteins positively regulate brassinosteroid signaling by stabilizing BRASSINOSTEROID INSENSITIVE1 at the plasma membrane.**

Luyao Li[1,†], Dexian Luo[1†], Chengzhu Yin[1,†], Chunyan Yan[1], Isabelle Vanhoutte[2,3], Yan Li[1], Bingbing Tang[1], Guorong Xiao[1], Xinyuan Feng[1], Wenhui Cao[1], Yong Wang[1], Eugenia Russinova[2,3,*], Derui Liu[1*]

[1] State Key Laboratory of Wheat Improvement, College of Life Sciences, Shandong Agricultural University, Tai'an, Shandong 271018, China

[2] Department of Plant Biotechnology and Bioinformatics, Ghent University, 9052 Ghent, Belgium

[3] Center for Plant Systems Biology, VIB, 9052 Ghent, Belgium

* Author for correspondence: eugenia.russinova@psb.vib-ugent.be (E.R.), drliu@sdau.edu.cn (D.L.)

† These authors contributed equally.

The author(s) responsible for distribution of materials integral to the findings presented in this article in accordance with the policy described in the Instructions for Authors (https://academic.oup.com/plcell/pages/General-Instructions) are: Derui Liu (drliu@sdau.edu.cn) and Eugenia Russinova (Eugenia.Russinova@psb.vib-ugent.be).

**Short Title**: 14-3-3 proteins stabilize BRI1 at the PM

**One Sentence Summary**: 14-3-3s stabilize BRI1 by antagonizing its ubiquitination

**Abstract**

Brassinosteroid (BR) hormones regulate various physiological and developmental processes in plants. BR signaling is primarily influenced by the abundance of the BR receptor BR INSENSITIVE1 (BRI1) at the plasma membrane, a process regulated by ubiquitination, endocytosis, and protein degradation. Despite extensive research, only a few negative regulators of BRI1 internalization and ubiquitination have been identified. In this study, we show that 14-3-3 proteins, which are conserved regulatory proteins in eukaryotes, directly interact with BRI1 at Threonine 872 (T872) within its juxtamembrane domain. In addition, Serine 858 (S858) in the juxtamembrane domain of BRI1 positively affects the phosphorylation status of T872, thereby contributing to the binding of 14-3-3 proteins to BRI1. Consequently, without altering the kinase activity of BRI1 or its interaction with the co-receptor BRI1-ASSOCIATED RECEPTOR KINASE1 (BAK1), but by inhibiting BRI1 ubiquitination, the binding of 14-3-3 proteins increased the abundance of BRI1 at the plasma membrane and enhanced BR signaling. Both non-epsilon and epsilon isoforms of 14-3-3 proteins contribute to the regulation of BRI1 and, consequently, to plant responsiveness to BRs. Our results reveled a previously undescribed function of 14-3-3 proteins in regulating BRI1 stability and, in turn, positively influencing BR signaling.

Key words: Arabidopsis, 14-3-3 protein, stability, endocytosis, BRI1

## Introduction

Brassinosteroids (BRs) are steroidal phytohormones that are essential for plant growth, development, and response to abiotic and biotic stresses (Nolan et al., 2020). BR signaling is initiated by the binding of the hormone to its plasma membrane (PM)-localized cognate receptor kinase (RK), BR INSENSITIVE1 (BRI1) (Friedrichsen et al., 2000; He et al., 2000) and its homologs, BRI1-LIKE1 (BRL1) and BRL3 (Caño-Delgado et al., 2004; Kinoshita et al., 2005). In the absence of BRs, the inhibitory protein BRI1 KINASE INHIBITOR1 (BKI1) (Wang and Chory, 2006; Jaillais et al., 2011; Jiang et al., 2015) primarily maintains BRI1 in an inactive state. However, upon binding to BRs, BRI1 heterodimerizes with its co-receptor BRI1-ASSOCIATED KINASE1 (BAK1), also known as SOMATIC EMBRYOGENESIS RECEPTOR KINASE3 (SERK3) and its homologs SERK1 and SERK4. During this process, BRI1 and BAK1 auto- and trans-phosphorylate to form fully activated receptor (Wang et al., 2008). BR binding to BRI1 also triggers dissociation of its negative regulators, BKI1 and BOTRYTIS-INDUCED KINASE1 (BIK1) (Wang et al., 2011; Lin et al., 2013). The BR signal is transduced from the PM to the nucleus through a sequential phosphorylation and dephosphorylation cascade to ultimately dephosphorylate and activate the master transcription factors, BRASSINAZOLE-RESISTANT1 (BZR1) and BRI1-EMS-SUPPRESSOR1 (BES1)/BZR2, which further control BR-responsive gene expression (Nolan et al., 2020).

The key determinant of BR signaling is the abundance of BRI1 in the PM, which is controlled by its ubiquitination, endocytosis and degradation (Di Rubbo et al., 2013; Gadeyne et al., 2014; Martins et al., 2015; Zhou et al., 2018; Liu et al., 2020). Ligand-dependent activation and phosphorylation of BRI1 promotes its association with the plant U-box (PUB) E3 ubiquitin ligases PUB12 and PUB13, which in turn directly ubiquitinate BRI1. Importantly, PUB13 is phosphorylated by BRI1 on a specific residue, enhancing their association. The ubiquitinated BRI1 is subsequently endocytosed and sorted for vacuolar degradation (Martins et al., 2015; Zhou et al., 2018). The ubiquitination of BRI1 can be alleviated by deubiquitinating enzymes UBP12 and UBP13, thereby stabilizing it (Luo et al., 2022). In addition to ubiquitination-dependent endocytosis, BRI1 regulates its PM pool through clathrin-mediated endocytosis (Di Rubbo et al., 2013; Gadeyne et al., 2014; Liu et al., 2020), which involves the adaptor protein complex-2 (AP-2) and TPLATE complex (TPC), as well as clathrin-independent endocytosis (Wang et al., 2015),

occurring with or without BR binding (Geldner et al., 2007; Claus et al., 2023).

14-3-3 proteins (hereafter 14-3-3s), also known as general regulatory factors (GRFs), are a family of regulatory proteins that are highly conserved in eukaryotes (Darling et al., 2005). Although they do not confer enzymatic activity, they function as dimers, with each monomer binding to phosphorylated (p) serine (S) or threonine (T) residues within their target proteins, making 14-3-3s also known as bridging proteins for protein-protein interactions. Three sequence-specific motifs, RSxpSxP, RSxxpSxP, and YpT, are the common phosphorylated peptides for 14-3-3 binding. However, 14-3-3s can also interact with phosphorylated proteins lacking these conserved motifs (Paul et al., 2012). Furthermore, although rare, phosphorylation-independent interactions with 14-3-3s have also been reported (Wang et al., 1999; Fuglsang et al., 2003).

The *Arabidopsis thaliana* (Arabidopsis) genome encodes 13 14-3-3 isoforms, which based on their sequence characteristics, are divided into two subfamilies: non-epsilon, including GRF1 to GRF8, and epsilon, including GRF9 to GRF13 (Denison et al., 2011). Although 14-3-3 isoforms share protein structural similarities and some functional redundancy, their targets and physiological functions may differ due to differences in spatiotemporal pattern of gene expression and subcellular localization (Alsterfjord et al., 2004; Paul et al., 2012; Keicher et al., 2017).

14-3-3s interact with numerous proteins to regulate their enzymatic and binding activity (Yang et al., 2019), subcellular localization (Gampala et al., 2007; Wang et al., 2011; Keicher et al., 2017), and turnover (Qi et al., 2022). In the presence of BRs, 14-3-3s bind to BKI1 to promote its dissociation from BRI1 at the PM (Jaillais et al., 2011; Jiang et al., 2015), making 14-3-3s positive regulators in BR signaling. However, in the absence or low concentration of BRs, 14-3-3s act as negative regulators by binding the phosphorylated BES1 and BZR1 in the cytoplasm, thereby decreasing their nuclear abundance (Gampala et al., 2007). High-throughput proteomics revealed that in Arabidopsis besides BES1, BZR1 and BKI1, the GRF2 isoform associates with several BR signaling components, including BRI1, BAK1, the phosphatase *bri1*-SUPPRESSOR1 (BSU1) (Chang et al., 2009), and the GSK3-like kinase BR-INSENSITIVE2 (BIN2) (Kim et al., 2023). In addition, 14-3-3s have been shown to interact directly with SERK1 (Rienties et al., 2005).

Although studies have hinted at an association between 14-3-3s and BRI1, the molecular mechanism of their interactions was only studied *in vitro* (Chae et al., 2016; Obergfell et al., 2024). Isothermal Titration Calorimetry (ITC) and site-directed mutagenesis of synthetic peptides were used to demonstrate that BRI1 strongly binds the non-epsilon 14-3-3 isoforms Chi (χ; GRF1),

Omega (ω; GRF2), Psi (ψ; GRF3) Phi (φ; GRF4), and Upsilon (υ; GRF5) (Chae et al., 2016) and that 14-3-3s recognize sequence-specific motifs in BRI1, BKI1, and BZR1 (Obergfell et al., 2024). As quadruple non-epsilon 14-3-3 mutants including *grf1,4,6,8*, *grf5,6,7,8*, and *grf1,4,5,7* exhibited BR hypersensitivity, 14-3-3s were considered to function mainly as negative regulators of BR signaling (Obergfell et al., 2024). In contrast, hypersensitivity to BRs resulting from *BRI1* overexpression was reduced in the triple *grf3,4,10* mutant (Lee et al., 2020). These findings imply that the roles of 14-3-3s in BR signaling are complex. Nevertheless, our understanding of how 14-3-3s regulate BRI1 is limited, and the physiological impact of 14-3-3s on BR signaling from the perspective of BRI1 remains elusive.

Here, we demonstrate that all ubiquitously expressed Arabidopsis 14-3-3s directly bind to BRI1 possibly at S858 and T872 residues in its juxtamembrane domain. Mutating S858 and T872 to alanine resulted in increased ubiquitination and degradation of BRI1, along with enhanced endocytosis and vacuolar targeting. Additionally, both non-epsilon and epsilon higher-order mutants, as well as RNAi plants, exhibited BRI1 instability and reduced sensitivity to BRs. Together, our findings establish 14-3-3s as positive regulators of BRI1 stability and, in turn, of BR signaling.

## Results

### 14-3-3s bind directly BRI1

Given that some 14-3-3 isoforms have been shown to associate with BRI1 and to confer specificity (Chang et al., 2009; Chae et al., 2016; Obergfell et al., 2024), we first tested whether isoforms co-expressed with BRI1 can interact. Of all the isoforms, *GRF1* to *GRF11* are ubiquitously expressed, which are very similar to the expression pattern of *BRI1* (Keicher et al., 2017). In contrast, *GRF12* is only expressed in flowers, and the expression level of *GRF13* is strikingly low (Wilson et al., 2016; Keicher et al., 2017). Therefore, GRF1 to GRF11 were selected for further analysis.

To determine whether GRFs interact directly with BRI1, we performed *in vitro* glutathione S-transferase (GST) pull-down assays using the bacterially expressed GST-tagged BRI1-cytoplasmic domain (CD), namely GST-BRI1-CD, and HIS-tagged GRFs. GST-BRI1-CD pulled down all GRF isoforms tested. The interaction between BRI1-CD and GRF2, GRF5, GRF6, GRF8, GRF9, and GRF11 was the strongest, between BRI1 and GRF3, GRF4, and GRF10 moderate, and

weak for GRF1, and GRF7, whereas no interactions were detected between GST (negative control) and each HIS-GRF3, HIS-GRF6, and HIS-GRF9 (Fig. 1A).

To verify the association between BRI1 and GRFs *in planta*, co-immunoprecipitation (co-IP) assays were carried out by transient expressing HA-tagged BRI1 together with the GFP-tagged isoforms GRF2, GRF3, GRF5, GRF6, GRF9, GRF10, and GRF11 or free GFP in *Nicotiana benthamiana* leaves. BRI1 associated with all tested GRFs, but not with free GFP (Fig. 1B). For further analysis we selected GRF6 to represent all GRFs as this non-epsilon isoform is the closest homolog of the epsilon group (Obergfell et al., 2024). To further confirm the direct interaction between BRI1 and GRF6, we performed mating-based split-ubiquitin (mbSUS) assay. Yeast cells transformed with *pBT3-STE-BRI1* and *pPR3N-GRF6* grew on SD-TLHA selective medium, whereas those transformed with the negative controls did not (Fig. 1C). Altogether our data demonstrate that probably all GRFs can bind BRI1 directly.

**GRF6 binds BRI1 at S858 and T872 in the juxtamembrane domain**

Because the BRI1-CD used in the pull-down assays (Fig. 1A) contained a juxtamembrane domain (JM), a kinase domain (KD), and a C-terminal domain (CTD), we sought to investigate which domain is sufficient to mediate BRI1 interaction with GRF6. To that aim, we performed pull-down assays by using different truncations of BRI1 fused to GST and HIS-GRF6. GRF6 was pulled down by BRI1-JK, containing both JM and KD, but not by BRI1-KC, containing both KD and CTD, or BRI1-K, containing only the KD domain, which indicates that the JM of BRI1 mediates a direct interaction with GRF6 (Fig. 2, A and B).

To validate the importance of JM for the BRI1-GRF6 interaction, a ratiometric bimolecular fluorescence complementation (rBiFC) assay was carried out in *Nicotiana benthamiana* (Grefen and Blatt, 2012). C-terminally tagged BRI1 (fused with the C-terminal fragment of yellow fluorescent protein, cYFP) combined with C-terminally tagged BKI1 (fused with the N-terminal fragment of YFP, nYFP) was used as a positive control (Liu et al., 2020). C-terminally tagged GRF6 (GRF6-nYFP) was combined with C-terminally tagged BRI1 or BRI1 with JM deletion ($BRI1^{\Delta JM}$). BKI1-nYFP/BRI1-cYFP, GRF6-nYFP/BRI1-cYFP, and GRF6-nYFP/$BRI1^{\Delta JM}$-cYFP exhibited strong, weak, and no interactions, as indicated by the YFP/RFP signal ratios, respectively (Fig. 2, C and D). Thus, deletion of the JM in BRI1 abolished its interaction with GRF6 *in vivo*, confirming the findings of the GST pull-downs (Fig. 2B). Notably, higher laser power and more

open pinhole were used to monitor the association between GRF6 and BRI1$^{\Delta JM}$ (Fig. 2C), under which condition chloroplast autofluorescence was also detected.

Most 14-3-3 targets contain motif(s) characterized by the amino acid sequences R/KSXpSXP (mode I), R/KXY/FXpSXP (mode II), or pS/pTx(1-2)-COOH (mode III) (Johnson et al., 2010). To identify the residue(s) that mediate(s) BRI1 interaction with GRF6 in JM, we looked for potential 14-3-3 binding motifs. S858, T872, and T880 had previously been identified as phosphorylated residues *in vitro* and *in vivo* (Wang et al., 2005, 2008), of which S858 and T872 and the surrounding residues, VKEAL(p)S858INLAA and PLRKL(p)T872FADLL, match the cargo recognition motif of 14-3-3s. ITC experiments with GRF8 and synthetic BRI1 peptides containing these motifs revealed that GRF8 only binds the phosphorylated RKL(p)T872FA motif, but not the phosphorylated KEAL(p)S858IN motif, nor the nonphosphorylated peptides (Obergfell et al., 2024). Although only (p)T872 was identified as GRF8 recognition site, because 14-3-3s form dimers to bind to their client protein at two sites, as in the case for BZR1 (Gampala et al., 2007) and BKI1 (Wang et al., 2011), it is still possible that both S858 and T872 are required for 14-3-3s to bind BRI1 *in vivo*.

To confirm the importance of S858 and T872, we first performed mbSUS assay by combining GRF6 with wild-type BRI1 or BRI1 with S858 and T872 mutated to alanine (A), namely BRI1$^{S858A;T872A}$ (Fig. 2E). Yeast cells containing pBT3-STE-BRI1$^{S858A;T872A}$ and pPR3-N-GRF6 did not grow on SD-LTAH medium, but in contrast, cells containing pBT3-STE-BRI1 and pPR3-N-GRF6 (positive control) were viable. To verify the involvement of S858 and T872 in the BRI1-GRF6 interaction in Arabidopsis, we introduced the C-terminally tagged with mCitrine (mCit) BRI1$^{S858A;T872A}$ mutant into the *bri1* null mutant, and use *pBRI1:BRI1-mCit/bri1* (Martins et al., 2015) as the control. GRF6-HA was further super transformed into homozygous *pBRI1:BRI1-mCit/bri1* and *pBRI1:BRI1*$^{S858A;T872A}$*-mCit/bri1* lines, which were used for co-IP assays. The association between GRF6 and BRI1 was weakened by the double S858A and T872A mutation (Fig. 2F).

As full activation of BRI1 in the presence of BRs relies on its kinase activity and association with BAK1 (Wang et al., 2001, 2008; Li et al., 2002; Nam and Li, 2002), we examined the effect of the S858A and T872A mutations on BRI1 kinase activity and BRI1-BAK1 association. The recombinant BRI1-CD mutant protein (GST-BRI1$^{S858A;T872A}$-CD) was compared with the wild-type BRI1 and the kinase-inactive BRI1$^{K911E}$-CD mutant for its ability to autophosphorylation

using anti-phosphoserine and threonine (α-pS/T) and anti-phosphotyrosine (α-pY) antibodies (Supplementary Fig. S1A). The BRI1$^{S858A;T872A}$-CD mutant behaved similarly to the wild-type BRI1-CD. Notably, the single BRI1$^{S858A}$-CD migrated faster than the BRI1-CD resembling the kinase inactive BRI1$^{K911E}$-CD mutant (Supplementary Fig. S1B), whereas the T872A mutation was previously shown to increase the kinase activity of BRI1 (Wang et al., 2005). We thus concluded that the two S858 and T872 phosphorylation sites are interdependent and hence they both might be required for the 14-3-3 recognition and binding *in vivo*.

Next, using the GST pull-down assay, we demonstrated that BRI1 and BRI1$^{S858A;T872A}$ bind to BAK1 to almost the same extent (Supplementary Fig. S2A). As a verification in Arabidopsis, we performed co-IP assays in the *pBRI1:BRI1-mCit/bri1* and *pBRI1:BRI1*$^{S858A;T872A}$*-mCit/bri1* lines. To trigger the interaction between BRI1 and BAK1, the seedlings were first treated with a BR biosynthesis inhibitor, brassinazole (BRZ), and then with the most biologically active BR, brassinolide (BL). The associations between BRI1 and BAK1, as well as between BRI1$^{S858A;T872A}$ and BAK1, were comparable (Supplementary Fig. S2B). Taken together, the impaired 14-3-3 binding did not interfere with the BRI1 kinase activity or the BRI1-BAK1 interaction. Accordingly, these data imply that both S858 and T872 phosphorylation sites contribute to GRF6 binding to BRI1.

We next tested whether 14-3-3 binding to BRI1 has any effect on its association with BAK1 and phosphorylation of BAK1. We performed co-IP assays by using *pBRI1:BRI1-mCit/bri1* and *p35S:GRF6-HA*;*pBRI1:BRI1-mCit/bri1* seedlings (Supplementary Fig. S3A). Intriguingly, the presence of GRF6 did not influence the association between BRI1 and BAK1 in the presence of BL (Supplementary Fig. S3A). BRI1 kinase activity was measured by incubating GST-BRI1-CD or HIS-BAK1$^{K317E}$-CD with or without HIS-GRF6. As detected by α-pS/T IB, the signal intensity of phosphorylated BAK1$^{K317E}$-CD in the presence of HIS-GRF6 was similar to that without GRF6 (Supplementary Fig. S3B), indicating that GRF6 binding to BRI1 does not affect BRI1 kinase activity or its association with BAK1.

**Interference with 14-3-3 binding sites in BRI1 compromised BR signaling**

To determine the effect of the S858A and T872A mutations on BR signaling, two homozygous *pBRI1:BRI1*$^{S858A;T872A}$*-mCit/bri1* lines (lines 3-3 and 7-3) with *BRI1* transcript levels comparable to or higher than that of the complemented *pBRI1:BRI1-mCit/bri1* line (Fig. 3A) were selected for

phenotypic analysis. Surprisingly, BRI1$^{S858A;T872A}$ protein levels were reduced when compared to that of the control (Fig. 3B), suggesting that BRI1 protein stability may be impaired by the S858A and T872A mutations. Consistently, *bri1* was only partially complemented by the *pBRI1:BRI1*$^{S858A;T872A}$*-mCit* construct as shown by the reduced rosette leaf area (Fig. 3C).

For quantification of BR sensitivity of the transgenic lines, the length of dark-grown hypocotyls in the presence of BL was measured. Both lines 3-3 and 7-3 were less sensitive to BL at concentrations of 10, 100, and 1000 nM than the control (Fig. 3D). Dephosphorylation of BES1 by exogenous BL is commonly used as a BR signaling activation readout (Yin et al., 2002). In agreement with the hypocotyl growth assay results, application of BL at 100 nM and 1000 nM for 1 h, dephosphorylated BES1 (dpBES1) to a lesser extent in lines 3-3 and 7-3 than in the control (Fig. 3, E and F). Collectively, the *pBRI1:BRI1*$^{S858A;T872A}$*-mCit/bri1* lines were less sensitive to exogenous BRs probably due to the reduced PM levels of BRI1 (Fig. 3, D and E).

**Depletion of 14-3-3 binding in BRI1 led to BRI1 polyubiquitination**

BRI1 undergoes polyubiquitination directly mediated by PUB12 and PUB13 (Zhou et al., 2018) and is further degraded in the vacuole (Martins et al., 2015). The proteasome inhibitor MG132 may stabilize BRI1, as BRI1-PUB13 association was more obvious in the presence of MG132 (Zhou et al., 2018). MG132 also stabilized BRI1$^{S858A;T872A}$ as that for BRI1 in the complemented line (Fig. 4A), reflecting, to some extent, the transcript levels of *BRI1*$^{S858A;T872A}$ or *BRI1* in each line (Fig. 3A). This indicates that the impaired protein stability for BRI1$^{S858A;T872A}$ may be a result of stronger ubiquitination modification than the wild-type BRI1.

To determine BRI1$^{S858A;T872A}$ ubiquitination level, we immunoprecipitated BRI1 (or BRI1$^{S858A;T872A}$)-mCit from the three lines by using the isolated microsomal fractions and probed them with α-ubiquitin antibodies (Fig. 4B). An increased molecular mass smear of approximately 100–250 kDa was detected in all samples, corresponding to polyubiquitinated BRI1. Corresponding with the decreased BRI1 stability for BRI1$^{S858A;T872A}$ and measured by the relative signal intensity ratio between ubiquitinated BRI1 (Ubn-BRI1) and immunoprecipitated BRI1, the BRI1 ubiquitination intensity was stronger in the two *pBRI1:BRI1*$^{S858A;T872A}$*-mCit/bri1* transgenic lines than in the control. The ratio between the ubiquitination of BRI1 and the total BRI1 protein ($Ub_n$-BRI1/BRI1-mCit) was 2-fold and 1-fold higher in lines 3-3 and 7-3, respectively (Fig. 4B).

BRI1 polyubiquitination is mediated by PUB12 and PUB13. To investigate the connection between 14-3-3 binding to BRI1 and PUB13-mediated BRI1 ubiquitination, we overexpressed PUB13-HA in *pBRI1:BRI1-mCit;bri1* and *pBRI1:BRI1*$^{S858A;T872A}$*-mCit/bri1* (#7-3) (Fig. 4D). Compared with *p35S:PUB13-HA/pBRI1:BRI1-mCit;bri1* plants, most *p35S:PUB13-HA/pBRI1:BRI1*$^{S858A;T872A}$*-mCit;bri1* (#7-3) plants exhibited a *bri1*-like phenotype (Fig. 4C and 4D), suggesting that BRI1$^{S858A;T872A}$ is hypersensitive to PUB13 overexpression, and that BRI1$^{S858A;T872A}$ may be degraded more than the wild-type BRI1 in a PUB13-dependent manner.

**Absence of 14-3-3 binding destabilized BRI1 in the plasma membrane**

As ubiquitination of BRI1 regulates its endocytosis (Martins et al., 2015; Zhou et al., 2018) and the S858A and T872A mutations increased BRI1 ubiquitination (Fig. 4B), we examined whether the PM and vacuole targeting of BRI1$^{S858A;T872A}$ were altered. To this end and because the fluorescence signals were too weak to be detected in the *pBRI1:BRI1*$^{S858A;T872A}$*-mCit/bri1* and *pBRI1:BRI1-mCit/bri1* lines, we generated overexpression lines expressing BRI1-GFP and BRI1$^{S858A;T872A}$-GFP from the *35S* promoter. We evaluated the expression level of BRI1 (or BRI1$^{S858A;T872A}$)-GFP and selected two lines for each construct with comparable expression levels for further characterization (Supplementary Fig. S4A). Both *p35S:BRI1-GFP*/Col-0 and *p35S:BRI1*$^{S858A;T872A}$*-GFP*/Col-0 lines display phenotypes of enhanced BR signaling (Supplementary Fig. S4B). But, no obvious differences were observed between *p35S:BRI1-GFP*/Col-0 and *p35S:BRI1*$^{S858A;T872A}$*-GFP*/Col-0 lines (Supplementary Fig. S4B).

Next, to determine whether the mutation would increase BRI1 internalization, we utilized several chemical treatments. Using cycloheximide (CHX) to inhibit *de novo* protein synthesis, we assessed the PM pool of BRI1 in the root meristem of 5-day-old seedlings. The ratio of PM to intracellular fluorescence intensity in *p35S:BRI1*$^{S858A;T872A}$*-GFP*/Col-0 plants was significantly lower than that in *p35S:BRI1-GFP*/Col-0 seedlings (Fig. 5, A and B), suggesting an increase in intracellular BRI1$^{S858A;T872A}$.

By passing through the trans-Golgi network/early endosomes (TGN/EEs), internalized BRI1 is targeted to vacuoles for degradation or recycled back to the PM (Irani et al., 2012). To better visualize the internalized BRI1, we took advantage of another chemical Brefeldin A (BFA) to inhibit endosomal trafficking, which leads to the accumulation of PM proteins in BFA bodies (Geldner et al., 2001). Consistent with the increased intracellular BRI1$^{S858A;T872A}$ (Fig. 5, A and B),

the GFP signal in BFA bodies was stronger in the BRI1$^{S858A;T872A}$-GFP than that in BRI1-GFP seedlings, as indicated by larger BFA bodies (Fig. 5, C and D).

To prevent BRI1 degradation in vacuoles (Martins et al., 2015), we applied Concanamycin A (ConcA), a vacuolar ATPase inhibitor, which allows visualization of accumulated BRI1-GFP or BRI1$^{S858A;T872A}$-GFP in vacuoles. ConcA treatment induced a dramatic accumulation of BRI1$^{S858A;T872A}$-GFP in the vacuole compared to BRI1-GFP (Fig. 5E), thus revealing an enhanced vacuolar delivery of BRI1$^{S858A;T872A}$ that may be triggered by ubiquitination modification. In addition to the GFP signal enhancement in vacuoles, larger ConcA bodies were present in *p35S:BRI1*$^{S858A;T872A}$*-GFP*/Col-0 than in *p35S:BRI1-GFP*/Col-0 seedlings (Fig. 5E).

**Octuple *grf1,2,3,4,5,6,7,8* mutant was hyposensitive to BRs**

To gain further insight into the function of 14-3-3s in BR signaling we used a quadruple *grf1,4,6,8* mutant also known as *klpc* (van Kleeff et al., 2014) (Supplementary Fig. S5A), in which Kappa (κ; *GRF8*), Lambda (λ; *GRF6*), Phi (φ; GRF4), and Chi (χ; GRF1) non-epsilon isoforms are mutated, hereinafter referred to as *grf1,4,6,8* (Supplementary Fig. 5A). The rosette of *grf1,4,6,8* mutant was smaller than that of the wild-type (Supplementary Fig. 5C), but the abundance of BRI1 in *grf1,4,6,8* was not altered (Fig. 6A). Considering the possible functional redundancy of 14-3-3s, and the ubiquitous expression of the non-epsilon isoforms suggesting low specificity (Keicher et al., 2017), we applied the CRISPR-Cas9 genome editing strategy to generate higher-order mutants in the *grf1,4,6,8* background. To reduce the risk of low editing efficiency, we designed two gRNAs for each of the remaining four non-epsilon GRFs, *GRF2*, *GRF3*, *GRF5*, and *GRF7*, and introduced the genome-editing cassette into *grf1,4,6,8*. From the mutant library, we succeeded in obtaining an octuple *grf1,2,3,4,5,6,7,8* mutant, creating pre-mature terminations in *GRF2*, *GRF5*, and *GRF7* and a 6-bp deletion in *GRF6* leading to 2 amino acid deletion (Supplementary Fig. 5B).

The *grf1,2,3,4,5,6,7,8* plants were even smaller than the *grf1,4,6,8* mutant (Supplementary Fig. 5C), phenocopying a weak *bri1* mutant. In contrast to *grf1,4,6,8*, the protein amount of BRI1 was clearly reduced in *grf1,2,3,4,5,6,7,8* (Fig. 6A), which was not a result of reduced *BRI1* transcription (Supplementary Fig. 5D). To characterize BRI1 internalization behavior, we overexpressed *p35S:BRI1-GFP* in *grf1,2,3,4,5,6,7,8*. We further assessed the PM pool of BRI1 in the root meristem of 5-day-old seedlings after CHX treatment. The ratio of PM to intracellular fluorescence intensity in *BRI1-GFP/grf1,2,3,4,5,6,7,8* seedlings was lower than that in *p35S:BRI1-*

*GFP*/Col-0 seedlings (Fig. 6, B and C), indicating an increase in BRI1 internalization in *BRI1-GFP/grf1,2,3,4,5,6,7,8*, and the reason for impaired BRI1 protein stability in *grf1,2,3,4,5,6,7,8*.

In line with the reduced BRI1 stability, *grf1,2,3,4,5,6,7,8* seedlings were less sensitive to 1000 nM BL than the wild-type seedlings, as determined by measuring the hypocotyl length of the dark-grown seedlings in the presence of increasing concentration of BL (Fig. 6, D and E). In addition, the accumulation of dephosphorylated BES1 was lower in *grf1,2,3,4,5,6,7,8* than that in wild-type after application of 100 and 1000 nM BL for 1 h (Fig. 6, F and G). These BR signaling phenotypes of *grf1,2,3,4,5,6,7,8* resembled those of the *pBRI1:BRI1*$^{S858A;T872A}$*-mCit/bri1* lines (Fig. 3, D and E).

**Knocking-down the expression of *GRF9*, *GRF10*, and *GRF11* destabilizes BRI1**

Given that the epsilon isoforms Mu (μ; GRF9), Epsilon (ε; GRF10), and Omicron (ο; GRF11) can also bind BRI1 (Fig. 1, A and B), and that they are also ubiquitously expressed (Keicher et al., 2017), we wondered whether they might also affect BRI1 stability in the same manner as the non-epsilon isoforms. To verify this hypothesis, we used an ethanol-inducible amiRNA line, called *emo* (Keicher et al., 2017), in which the 14-3-3 isoforms *GRF9*, *GRF10* and *GRF11* are knocked down by an ethanol treatment, hereinafter referred to as *grf9,10,11*$^{RNAi}$ (Supplementary Fig. S6A), whereas *BRI1* transcript levels remained unaffected (Supplementary Fig. S6B). Soil-grown ethanol-treated wild-type plants were only slightly smaller, but ethanol-treated *grf9,10,11*$^{RNAi}$ plants were visibly smaller than those without treatment (Supplementary Fig. S6C). Similar to that in *grf1,2,3,4,5,6,7,8*, BRI1 protein level was lower in ethanol-treated *grf9,10,11*$^{RNAi}$ than in the mock, whereas those in wild-type remained unchanged (Fig. 7A). To verify that BRI1 protein stability also relies on the expression of *GRF9*, *GRF10*, and *GRF11*, we transformed *pBRI1:BRI1-mCit* and *pBRI1:BRI1*$^{S85A8;T872A}$*-mCit* into *grf9,10,11*$^{RNAi}$ line by transformation. Lines with comparable BRI1-mCit and BRI1$^{S85A8;T872A}$-mCit were selected for further analysis. Similar to the endogenous BRI1 in *grf9,10,11*$^{RNAi}$, when *pBRI1:BRI1-mCit/grf9,10,11*$^{RNAi}$ was treated with ethanol, BRI1-mCit decreased. Interestingly, the BRI1$^{S858A;T872A}$-mCit levels were insensitive to the ethanol treatment (Fig. 7B) indicating that BRI1 stability governing mediated by GRF9,10, and 11 is through their binding at S858 and T872. The decreased BRI1 protein level in *grf9,10,11*$^{RNAi}$ under ethanol treatment is consistent with increased BRI1 ubiquitination (Fig. 7C). BRI1 instability

in ethanol-treated *grf9,10,11*$^{RNAi}$ could be alleviated by overexpressing GFP-tagged GRF6 (Fig. 7D), indicating that non-epsilon and epsilon 14-3-3s may redundantly stabilize BRI1.

## Discussion

Previous studies on the functions of 14-3-3s in BR signaling have mainly focused on BES1, BZR1 and BKI1. In this study, by mutating the 14-3-3 binding sites in BRI1, and using octuple mutant *grf1,2,3,4,5,6,7,8* and *grf9,10,11*$^{RNAi}$, we demonstrated that both non-epsilon and epsilon 14-3-3 isoforms bind and stabilize BRI1 by antagonizing the ubiquitination modification of BRI1. This, in turn, affected BRI1 ubiquitination and endocytosis. Moreover, a similar scenario of 14-3-3s regulating BRI1 and BR signaling may also exist for other RKs and RK-mediated signaling pathways. Thus, our findings may provide a new perspective on the modulation of RK signaling.

### 14-3-3s-BRI1-BAK1 complex formation, BRI1 ubiquitination and endocytosis

BRI1 heterodimerization with its co-receptor and the subsequent reciprocal transphosphorylation is the prerequisite for BR signal transduction, which requires their spacial proximity. Our *in vitro* and *in vivo* data all suggest that 14-3-3s do not sterically hinder BRI1 and BAK1 interaction. This speculation is supported by the predicted structures of BRI1-CD/BAK1-CD/GRF6 trimer by AlphaFold (Supplemental Figure S7B), as compared with BRI1-CD/BAK1-CD dimmer, the BRI1-BAK1 interface is only mildly changed in BRI1-CD/BAK1-CD/GRF6 trimer (Supplemental Figure S7). This could be explained by the fact that 14-3-3s bind to BRI1 at the juxta-membrane domain, but not the kinase domain. Since the 14-3-3s form dimers to further bind to their targets, these dimers may target the BRI1-BAK1 heterodimer in the presence of BRs. This hypothesis is supported by evidence showing that 14-3-3s can directly bind to the BAK1 homolog SERK1 (Rienties et al., 2005) and possibly interact with BAK1 in Arabidopsis (Chang et al., 2009). Several putative 14-3-3 binding motifs in the cytoplasmic domain of BAK1 and SERK1 were predicted, including BAK1$^{323-327}$, BAK1$^{600-610}$, SERK1$^{289-293}$, SERK1$^{412-417}$, and SERK1$^{566-576}$, using the eukaryotic linear motif (ELM) server (ELM - Search the ELM resource) (Puntervoll et al., 2003). But, the phosphorylation modification of $S_{325}$ and $S_{604}$ in BAK1, and $S_{291}$, $S_{415}$, and $S_{570}$ in SERK1, have not been reported yet. Thus, non-canonical 14-3-3 binding motifs may exist in BAK1 and SERK1.

BRI1 auto-phosphorylation is required for BRI1-BAK1 association and its full activation. Fully-activated BRI1 interacts with and phosphorylates the E3 ubiquitin ligases PUB12 and PUB13, which in turn ubiquitinate BRI1 for degradation, thus reducing BRI1 abundance at the PM (Zhou et al., 2018). Kinase activity may be necessary for BRI1 interaction with 14-3-3s, because the targeted residues of 14-3-3s must be phosphorylated (Obergfell et al., 2024). The association between GRF6 and the kinase-inactive form of BRI1, BRI1$^{K911E}$, was dramatically weaker than that with the wild-type BRI1, shown by the GST pull-down assay. Binding of 14-3-3s to BRI1 may antagonize PUB12 and PUB13-mediated ubiquitination of BRI1. BRI1 is K63 polyubiquitinated *in vivo*, and ubiquitination promotes its internalization and sorting for vacuolar degradation (Martins et al., 2015). One of the major ubiquitination sites in BRI1 is K866, adjacent to S858 and T872, the two 14-3-3s binding sites in BRI1, thus BRI1 polyubiquitination may be sterically hindered by 14-3-3 binding, and vice versa. It may explain the hypersensitivity of *pBRI1:BRI1*$^{S858A;T872A}$*-mCit/bri1* to PUB13 overexpression shown in our study.

Mutation of 14-3-3 binding sites in BRI1 enhanced its ubiquitination and internalization. The ubiquitination of BRI1 is well-known as a prerequisite for its ubiquitin-dependent endocytosis (Martins et al., 2015; Zhou et al., 2018). In addition, BRI1 undergoes AP-2- and TPC-dependent clathrin-mediated endocytosis (Di Rubbo et al., 2013; Gadeyne et al., 2014; Liu et al., 2020) as well as clathrin-independent endocytosis (Wang et al., 2015). Studies with the recently generated tool BRI1$^{Q}$, a BR binding-deficient mutant (Claus et al., 2023), further complicated our understanding of the endocytic machinery mediating BRI1 endocytosis. BRI1 endocytosis was enhanced in *grf1,2,3,4,5,6,7,8* mimicking the phenotype of BRI1$^{S858A;T872A}$ and the artificially ubiquitinated BRI1 (Martins et al., 2015). Regulation of endocytosis by 14-3-3s is not unique for BRI1, because endocytosis of PINOID2 was also enhanced in the *grf9,10*,11$^{RNAi}$ line (Keicher et al., 2017).

**Positive or negative regulators of 14-3-3s in BR signaling depends on where they act**

BR signaling is largely determined by the amount of functional BRI1 protein in the PM. Our study revealed that 14-3-3s stabilize BRI1 at PM and positively regulate BR signaling. However, whether 14-3-3s are general positive or negative regulators of BR signaling remains controversial. As, first, hypersensitivity to BRs resulting from *BRI1* overexpression was reduced in the *14-3-3* triple mutant *grf3,4,10* (Lee et al., 2020), indicating a positive role of 14-3-3s in BR signaling, and second, three

quadruple 14-3-3 mutants *grf1,4,6,8*, *grf5,6,7,8*, and *grf1,4,5,7* were weakly less sensitive to BRZ, suggesting that 14-3-3s are negative regulators of BR signaling (Obergfell et al., 2024). Noteworthy, BRZ sensitivity may not be a very clear readout of BR responses as it also affects BR biosynthesis, and BRZ insensitivity is also found in signalling deficient mutants including BR biosynthetic null mutant *cpd*, BR perception mutant *bri1-701*, and SERK triple-null mutant *serk1-8 bak1-4 bkk1-1*. It suggests that reduced BRZ sensitivity does not always equals to more BR signaling. These conflicting findings may be due to isoform binding specificity to a certain extent, for different targets including BRI1, BKI1, BES1, BZR1, and maybe even SERKs, although GRF8 was shown to bind the phosphorylated short linear motifs in BRI1, BKI1, and BES1 (Obergfell et al., 2024). The conflicting findings may mainly attribute to where 14-3-3s target to, as binding to BRI1, BKI1, or BES1/BZR1 resulting elevated or declined BR signaling. Almost all studies about 14-3-3s are from the non-epsilon isoforms, little was known about how epsilon group 14-3-3s contribute to BR signaling. In addition, their binding efficiency may differ between different 14-3-3 isoforms in terms of the same target.

Our GST pull-down and co-IP assays showed that all 14-3-3 isoforms could bind to BRI1. BRI1 protein levels were less abundant in both *grf1,2,3,4,5,6,7,8* and *grf9,10,11*$^{RNAi}$, and *GRF6* overexpression complemented the decreased BRI1 amounts in *grf9,10,11*$^{RNAi}$. These findings point to a potential redundancy between the non-epsilon and the epsilon 14-3-3 isoform for their recognition and stabilization of BRI1. This lack of isoform specificity has also been shown for the interaction between 14-3-3s and NON-PHOTOTROPIC HYPOCOTYL (Reuter et al., 2021). But this phenomenon may not be true for all 14-3-3 targets, as the early flowering phenotype shown in in the Flag-tagged BRI1 overexpressed plants in wild type background, lost in the triple *14-3-3* mutant *grf3,4,10*, could not be rescued by introducing any of the three isoforms (Lee et al., 2020). The same may exist for 14-3-3s isoforms binding BKI1, BES1, BZR1, and even SERKs.

Taken together, drawing a conclusion about whether14-3-3s are generally positive or negative regulators in BR signaling would be unnecessary and unrealistic, as it really depends on where 14-3-3 proteins target to.

**14-3-3s contribute to RK-mediated signaling and their function may also rely on RKs**

14-3-3s target to a large number of proteins in a variety of biological activities (Huang et al., 2021). RKs, as being phosphorylated are also potential targets of 14-3-3s. Large-scale and high throughput

interactome assays using each of the 14-3-3 isoforms will map out all the 14-3-3 and RK interaction. Starting from there, the biological functions of these interactions will be of interesting to investigate further.

14-3-3s themselves can be modified by phosphorylation, potentially affecting their sub-cellular localization and client binding (Liu et al., 2017; Aitken, 2011). BRI1 and BAK1 phosphorylate 14-3-3s in a BR-dependent manner (Chae et al., 2016), and the phosphorylation sites in GRF2 *in planta* has been revealed (Wu et al., 2011). Thus, there may be a feed-back forward effect between the association of 14-3-3s and BRI1 and BAK1 positively regulating BR signaling. Phosphorylated 14-3-3s may also target to other proteins thus participate in other signaling pathways. The crosstalk between BR signaling and others may partially rely on BRI1- and BAK1-mediated 14-3-3 phosphorylation.

## Materials and methods

### Plant materials and growth condition

Arabidopsis *thaliana* L. Heynh., accession Columbia 0 (Col-0) was used as the wild-type. *pBRI1:BRI1-mCit* expressed in *bri1* (*pBRI1:BRI1-mCit/bri1*), *bri1* null mutant (GABI_134E10), *grf1,4,6,8* and *grf9,10,11*$^{RNAi}$ were described previously (Jaillais et al., 2011; Martins et al., 2015; Zhou et al., 2018; van Kleeff et al., 2014; Keicher et al., 2017).

For phenotypic analysis, plants were grown in soil for 22-28 days at 22°C, 50-60% relative humidity, and a 16-h light/8-h dark regime, under a standard daytime light intensity (90 mmol/m$^2$/s) from full-spectrum fluorescent light bulbs. For growth on plates or in liquid medium, Arabidopsis seeds were sterilized with sodium hypochlorite and Triton X-100 and sown on plates with half-strength Murashige and Skoog (½MS) medium containing 0.5% (w/v) sucrose, 1% (w/v) agar, and 0.05% (w/v) MES, pH 5.7. After vernalization for 2 days at 4°C, the plates were transferred to the growth chamber at 22°C under a 16-h/8-h light/dark cycle or in the dark after 2 h of light for different periods of time, depending on the experiments. Plants were grown on plates for 6 days for the microsomal protein preparation; for 5 days for the BRI1 internalization assay, transcript analyses, protein abundance analysis, and dark-grown BR and ConcA sensitivity assays; for 4 h followed by 6 more days of treatment with different BL or ConcA concentrations. For Co-IP assays with seedlings, plants were grown on plates for 3 days, then transferred to ½MS liquid medium for

5 days, followed by treatment with BRZ (2 μM) for 3 days and BL (1 μM) for 90 min.

**Molecular cloning**

cDNA or genomic DNA from 5-day-old Col-0 seedlings or indicated vectors were used as templates for PCR cloning using the indicated primers listed in Supplementary Table S1. For transient expression in *Nicotiana benthamiana*, *pDONR221-BRI1* was recombined with the *35S* promoter and HA tag into the *pK7m34GW* vector (Karimi et al., 2007) to generate the *pK7m43GW-p35S:BRI1-HA*. The cDNA of *BRI1* was in-fusion cloned into *pCB302-p35S:2xFlag* digested with *Bam*HI and *Stu*I to generate *pCB302-p35S:BRI1-2xFlag*. The gDNA fragment of *GRF6* was cloned into *pDONR221* to generate *pDONR221-GRF6*, which was recombined with the *35S* promoter and *GFP* tag into the *pK7FWG2* to generate *pK7FWG2-p35S:GRF6-GFP*. The truncated version of BRI1 was built by amplification of $BRI1^{\Delta JM}$, the fragments comprising extracellular domain and transmembrane domain (ECD+TM), and the kinase domain and C-terminal domain (KD+CT) and cloned into *pUC19* with the LightNing™ DNA Assembly Mix Plus (iScience) to create *pUC19-BRI1*$^{\Delta JM}$. The cDNAs encoding *BKI1* or *GRF6* were cloned into *pDONR221-P3P2*, and *BRI1* (or *BRI1*$^{\Delta JM}$) into *pDONR221-P1P4*, which were further cloned into *pBiFC-2in1-CC* to generate *pBiFC-BKI1-nYFP-BRI1-cYFP*, *pBiFC-GRF6-nYFP-BRI1-cYFP*, and *pBiFC-GRF6-nYFP-BRI1*$^{\Delta JM}$*-cYFP*. The gDNA fragments of each of the 9 *GRFs* selected including *GRF2*, *GRF3*, *GRF5*, *GRF6*, *GRF9*, *GRF10*, and *GRF11*, were in-fusion cloned into *pCB302-p35S::GFP* digested with *Bam*HI and *Stu*I individually to generate the *pCB302-35S::GRF-GFP* constructs, individually.

For stable expression in Arabidopsis, *pDONR221-BRI1*$^{S858A;T872A}$ was obtained by site-directed mutagenesis with *pDONR221-BRI1* (Jaillais et al., 2011) as template. *pDONR221-BRI1*$^{S858A;T872A}$, *pDONRP4P1r-pBRI1*, and *pDONRP2rP3-mCitrine* were recombined into *pK7m34GW* to generate *pK7m34GW-pBRI1:BRI1*$^{S858A;T872A}$*-mCit*. The CDS fragments of WT *BRI1* and *BRI1*$^{S858A;T872A}$ were amplified using *pDONR221-BRI1* and *pDONR221-BRI1*$^{S858A;T872A}$ as templates. The fragments were in-fusion cloned into *pCB302-p35S:GFP* digested with *Bam*HI and *Stu*I to generate *pCB302-p35S:BRI1-GFP* and *pCB302-p35S:BRI1*$^{S858A;T872A}$*-GFP*. cDNA fragments of *GRF6* (or *GRF6*$^{4A}$) and *PUB13* were amplified by using *pET28a-GRF6*, *pET28a-GRF6*$^{4A}$ (Liu et al., 2017) or Col-0 cDNA as templates. The fragments were in-fusion cloned into *pMDC32-2xp35S:EGFP-HA* digested with *Bam*HI and *Stu*I to generate *pMDC32-2xp35S:GRF6*

(or *GRF6*$^{4A}$)-*HA* and *pMDC32-2xp35S:PUB13-HA*, respectively, or were ligated into *pZP211-p35S:3xFlag* digested with *Bam*HI and *Spe*I to generate *pZP211-p35S:GRF6* (or *GRF6*$^{4A}$)-*3xFlag*.

The clones used for protein expression were made as follows: the cDNAs encoding the *BRI1-CD*, *BRI1*$^{S858A;T872A}$*-CD*, *BRI1-JK*, *BRI1-KC*, and *BRI1-K* were in-fusion cloned into *pGEX4T-1* digested with *Bam*HI and *Sal*I to generate *pGEX4T-GST-BRI1-CD*, *pGEX4T-GST-BRI1*$^{S858A;T872A}$*-CD*, *pGEX4T-GST-BRI1-JK*, *pGEX4T-GST-BRI1-KC*, and *pGEX4T-GST-BRI1-K*, respectively. *pGEX4T-BRI1*$^{S858A}$*-CD* and *pGEX4T-BRI1*$^{K911E}$*-CD* were obtained by site-directed mutagenesis with *pGEX4T-BRI1-CD* as template. The cDNAs encoding the full length of selected *GRFs* and the *BAK1-CD* were in-fusion cloned into *pET28a* digested with *Bam*HI and *Sal*I to generate *pET28a-HIS-GRFs*, and *pET28a-HIS-BAK1-CD*, respectively. For the split-ubiquitin based Y2H experiment, full-length *BRI1* and *BRI1*$^{S858A;T872A}$ were restriction digested and ligated into *pBT3-STE* and *GRF6* into *pPR3-N* with *Sfi*I.

The *grf1,2,3,4,5,6,7,8* mutant was generated by disrupting *GRF2*, *GRF3*, *GRF5*, and *GRF7* simultaneously in the *grf1,4,6,8* background by means of the CRISPR-Cas9 genome editing technology. For each gene, two gRNAs were designed with the web tool CRISPOR (http://crispor.org) (Concordet and Haeussler, 2018). The eight sgRNAs targeting *GRF2*, *GRF3*, *GRF5*, or *GRF7* were cloned into a single CRISPR/Cas9 vector using the Golden Gate technology as previously described (Decaestecker et al., 2019). Briefly, the gRNA pairs were cloned into the Golden Gate entry modules *pGG-A-AtU6ccdB-B*, *pGG-B-AtU6ccdB-C*, *pGG-C-AtU6ccdB-D*, or *pGG-D-AtU6ccdB-E*. Four-armed entry vectors, each containing two sgRNAs, together with the *pGG-E-linker-G* vector were assembled into a CRISPR destination vector *pFASTRK-pRPS5Ap-AtCas9-NLS-P2A-mCherry-G7T-A-Cm*$^{R}$*-ccdB-G*.

**Generation of transgenic plants**

*Agrobacterium tumefaciens* (strain GV3101)-mediated transformation into the heterozygous *bri1* null mutant, Col-0, *grf9,10,11*$^{RNAi}$, *grf1,4,6,8*, *pBRI1:BRI1-mCit/bri1*, *pBRI1:BRI1*$^{S858A;T872A}$*-mCit/bri1*, or *p35S:BKI1-GFP*/Col-0 was used to create stable transgenic lines. The transformants were screened by germination on 0.6% (w/v) agar plates (without sucrose and with 100 mg/L timentin) containing 50 mg/L kanamycin, 10 mg/L BASTA, or 25 mg/L hygromycin according to the plant resistance marker in the binary vectors.

**Chemical treatments**

MG-132 (Cell Signaling Technology; 10 mM stock in DMSO), Brassinolide (Cayman; 10 mM stock in DMSO), Brassinazole (Macklin; 10 mM stock in DMSO), Brefeldin A (Psaitong; 50 mM stock in DMSO), CHX (Merck; 50 mM stock in DMSO), and Concanamycin A (Cayman; 115 μM stock in acetonitrile) were used at the concentrations indicated and plants were treated for the indicated periods.

**Recombinant protein expression, purification, and GST pull-down**

Fusion proteins were generated from bacterial protein expression vectors as described above in *Escherichia coli* BL21 or Rosetta strain grown in Luria-Bertani medium supplemented with 0.5 mM isopropyl β-D-1-thiogalactopyranoside and induced for 16 h at 16°C. The GST- or 6xHIS-fused proteins were purified with glutathione sepharose 4B GST-tagged protein purification resin (Solarbio) or His-tag protein purification kit (CWBIO), respectively, according to the manufacturers' standard procedures.

Approximately 10 μg of GST or GST-fused proteins in the pull-down buffer (20 mM Tris-HCl, pH 7.5, 100 mM NaCl, 0.1 mM EDTA, 0.2% [v/v] Triton X-100) were incubated with prewashed 20 μL glutathione agarose beads (Solarbio) at 4°C for 2 h with gentle shaking. Beads were washed with 400 μL pull-down buffer once, followed by incubation with 10 μg of 6xHIS-fused proteins by shaking at 4°C for another 1 h. Afterward, the beads were washed four times with 400 μL washing buffer (20 mM Tris-HCl, pH 7.5, 300 mM NaCl, 0.1 mM EDTA, 0.5% [v/v] Triton X-100). Beads were boiled in 50 μL of 2×SDS protein loading buffer for 5 min and detected by immunoblotting (IB) with a-GST (TRANS, X015, 1:3,000) and a-HIS (TRANS, E065, 1:3,000) antibodies. For blocking and antibody dilutions, 5% (w/v) nonfat milk powder in 0.1% (v/v) Tween-20 containing Tris-buffered saline (TBST) was used.

**Immunoblot analysis and co-immunoprecipitation**

For autophosphorylation analysis, equal amounts of recombinant GST-tagged wild-type, S858A;T872A-mutated, S858A-mutated, and kinase-dead ($BRI1^{K911E}$) BRI1-CD proteins were loaded and detected by IB with α-pS/T (ECM Biosciences, PP2551, 1:1,000), α-pY (Invitrogen, 10-5001-82, 1:3,000), α-$pS_{858}$ (Oh et al., 2012, 1:2,000) and a-GST antibodies. For *in vitro* kinase assay, 1 μg of GST-BRI1-CD was incubated with 10 μg HIS-tagged kinase-dead BAK1-

CD (HIS-BAK1$^{K317E}$-CD) with or without the presence of 2 μg HIS-GRF6 in kinase reaction buffer (10 mM Tris-HCl, pH 7.5, 5 mM $MgCl_2$, 2.5 mM EDTA, 50 mM NaCl, 0.5 mM dithiothreitol [DTT] and 50 μM ATP) at the final volume of 20 μL. After gentle shaking for 2 h at room temperature, samples were denatured by adding 5 μL 5×SDS loading buffer and boiled for 5 min. The samples were detected by IB with a-pS/T, a-GST, and a-HIS antibodies.

For the BRI1 and BAK1 expression and BES1 dephosphorylation assays, 5-day-old seedlings untreated or treated with 50 μM MG-132 or BL (10, 100, and 1000 nM) were pulverized and extracted with 2xSDS loading buffer and directly boiled for 10 min, followed by centrifugation at 13,000*g* for 10 min. The supernatants were detected by IB with α-GFP (TRANS, D044, 1:3,000), α-BRI1 (Agrisera, AS12 1859, 1:5,000), α-BAK1 (Agrisera, AS12 1858, 1:5,000), α-BES1 (Yin et al., 2002, 1:3,000), and β-ACTIN (CWBIO, CW0264, 1:10,000) antibodies. For BES1 dephosphorylation assays, the ratio of the dephosphorylated BES1 to the total BES1 was quantified based on the band intensity using ImageJ.

For co-IP in *N. benthamiana*, *A. tumefaciens* (strain LBA4404) expressing *p35S:BRI1-HA*, *p35S:GFP* or *p35S:GRF-GFP* for each of 7 *GRFs* selected were resuspended in infiltration buffer (10 mM $MgCl_2$, 10 mM MES pH 5.6, 0.1 mM acetosyringone) for 2 h at room temperature. *p35S:BRI1-HA* culture was mixed with *p35S:GFP* or each of the *p35S:GRF-GFP* to a final $OD_{600}$=0.5. Two days after infiltration into *N. benthamiana*, leaves were harvested, ground to powder with liquid nitrogen, and solubilized in extraction buffer [50 mM Tris-HCl, pH 7.5, 150 mM NaCl, 2.5 mM EDTA, 10% (v/v) glycerol, 1% (v/v) NP-40, 5 mM DTT, complete EDTA-free protease inhibitor cocktail (SIGMA)] in a 1:2 (w:v) for 30 min at 4°C with gentle shaking. The extracts were centrifuged twice at 16,000*g* at 4°C for 20 min and the supernatants were incubated with α-GFP-coated magnetic beads (AlpaLifeBio) or α-HA-coated magnetic beads (Beyotime) for 2 h at 4°C, followed by washing three times with 1 mL of washing buffer (same as extraction buffer but without protease inhibitor). Beads were eluted with 40 μL 2xSDS loading buffer and boiled for 10 min. Samples were analyzed by IB with α-GFP and α-HA (Beyotime, AF2858, 1:2,000) antibodies.

Arabidopsis microsomal fractions were isolated according to the published protocol (Liu et al., 2020) with the minor modification that seedlings were treated with only 50 μM MG-132 for 5 h. For co-IP with Arabidopsis rosette leaves as material, the same protocol was used as described above for co-IP in *N. benthamiana*. For solubilized microsomal fractions, the same co-IP protocol

was used as above, starting from incubation with the prewashed α-GFP-coated magnetic beads. Samples were analyzed by IB with α-GFP, α-HA, α-ubiquitin (Cell Signaling Technology, 3933S, 1:2,000), and α-Flag (TRANS, HT201, 1:3,000) antibodies.

For blocking and antibody dilutions, 5% (w/v) BSA powder in 0.1% (v/v) TBST was used for α-pS/T, α-pY, and α-$pS_{858}$ IBs, and TBST-containing 5% (w/v) nonfat milk powder for the remaining IBs.

**qRT-PCR**

Total RNA was extracted from 5-day-old seedlings with Ultrapure RNA kit (CWBIO). cDNA was synthesized with the EasyScript One-Step gDNA Removal and cDNA Synthesis SuperMix (TRANS). qRT-PCRs were run with TransStart Tip Green qPCR SuperMix Tip Green (TRANS) on a QuantStudio 6 Flex (Applied Biosystems, Thermo Fisher Scientific). The *BRI1* and *GRF* expressions were normalized to that of *ACTIN2*. The cycling conditions were as follows: 50°C, 2 min, and 95°C, 1 min (pre-incubation); 95°C, 15 s, and 60°C, 1 min (40 cycles of amplification); 95°C, 15 s, 60°C, 1 min, and 95°C, 15 s (melting curve).

**Split-ubiquitin based Y2H**

Constructs used for the Y2H assay were generated as described above. Plasmids with different combinations were co-transformed into the yeast strain NMY51 by the LiAc-mediated yeast transformation (Gietz and Schiestl, 2007). Positive yeast transformants were screened on SD/-Trp-Leu medium, and protein interactions were selected on SD/-Trp-Leu-His-Ade medium.

**Confocal imaging and data analysis**

For analysis of BRI1-GRF6 rBiFC, BRI1 internalization and and vacuole targeting, *N. benthamiana* leaves or the meristem zone of Arabidopsis roots were imaged with a 20x objective lens (numerical aperture, 0.8) or a 60x oil corrected immersion objective lens (numerical aperture, 1.4) on a confocal laser scanning microscope (LSM880; Zeiss). The excitation/emission wavelengths used were 488 nm/505-552 nm for GFP (or YFP) and 594 nm/605-639 nm for RFP. Images were converted to 8-bit in ImageJ for YFP and RFP intensity quantification in rBiFC assays, and for BRI1 (or $BRI1^{S858A;T872A}$)-GFP fluorescence signal intensity measurements. Regions of interest were selected based on the PM or cytosol localization. The averages of the top bright 10%

pixels from the whole PM or intracellular part were used to calculate the YFP/RFP ratios, or the relative PM/intracellular fluorescent intensity as previously described (Liu et al., 2020). BFA body size was measured as previously described (Luo et al., 2015).

**AlphaFold structure prediction**

The structural configurations of BRI1-CD/BAK1-CD and BRI1-CD/BAK1-CD/GRF6 were predict using AlphaFold (AlphaFold Server), a dedicated online server for protein three-dimentional structure prediction (Jumper et al., 2021).

**Quantification and Statistical Analysis**

Statistical analyses were carried out in Excel with build-in formulas or XL Toolbox NG. The *P* values were calculated with two-tailed Student's unpaired *t*-test analysis for binary comparison, or with one-way ANOVA and Tukey's post hoc honestly significance test for comparisons of more than two genotypes or combinations. The measurements shown in box plots display the first and third quartiles and are split by medians (center lines), with whiskers extending to 1.5-fold the interquartile range from the 25th and 75th percentiles. Outliers are represented by dots. The measurements shown in graphs display the averages and standard errors.

**Accession Numbers**

Sequence data from this article can be found in the GenBank/EMBL data libraries under accession numbers: BRI1 (At4G39400); GRF1 (AT4G09000); GRF2 (AT1G78300); GRF3 (AT5G38480); GRF4 (AT1G35160); GRF5 (AT5G16050); GRF6 (AT5G10450); GRF7 (AT3G02520); GRF8 (AT5G65430); GRF9 (AT2G42590); GRF10 (AT1G22300); GRF11 (AT1G34760); PUB13 (AT3G46510); BAK1 (AT4G33430); and BKI1 (AT5G42750).

**Author contributions**

D.Liu and E.R. initiated the project and designed experiments. L.L. generated most of the plant materials, most of the clones, and performed the kinase assays, B.L. treated growth assay, BES1 dephosphorylation assay, BRI1 stability assays, ConcA sensitivity assay, qRT-PCR analysis, most of the genotyping, and helped with co-IP assays. D.Liu generated the CRISPR constructs, the *grf1,2,3,4,5,6,7,8* mutant, and performed part of BR-related phenotypic analysis, most of the co-IP

assays, and part of the GST pull-down assays. C.Yin performed part of the co-IP assays, most of the Y2H assays, and part of GST pull-down assays. C.Yan performed part of the Y2H experiments. I.V. generated part of the plant materials. Y.L. and G.X. participated in the genotyping, co-IP assays, and part of the cloning work. B.T. performed the BAK1 stability assay, and part of protein purification. X.F. and W.C. participated in protein expression, purification, and GST pull-down assays. D.Liu performed BRI1 ubiquitination assay, and the confocal imaging and data analysis. Y.W. gave guidance on the writing and revision of the manuscript. E.R. and D.Liu wrote the manuscript. All authors revised the manuscript.

**Supplementary Data**

**Supplementary Figure S1**. Effect of S858A and T872A mutations on BRI1 kinase activity *in vitro*.

**Supplementary Figure S2**. BRI1 association with BAK1 was not affected by the S858A and T872A mutations in BRI1

**Supplementary Figure S3**. BRI1 association with BAK1 and BRI1 kinase activity were unaffected by the presence of GRF6.

**Supplementary Figure S4**. Characterization of *p35S:BRI1-GFP*/Col-0 and *p35S:BRI1*$^{S858A;T872A}$*-GFP*/Col-0 transgenic plants.

**Supplementary Figure S5**. Molecular characterization of the quadruple *grf1,4,6,8* mutant and octuple *grf1,2,3,4,5,6,7,8* mutant.

**Supplementary Figure S6**. Molecular characterization of the ethanol-inducible amiRNA line, *grf9,10,11*$^{RNAi}$.

**Supplementary Figure S7**. Three-dimensional structure of BRI1-CD/BAK1-CD dimmer and BRI1-CD/BAK1-CD/GRF6 trimer predited by AlphaFold.

**Supplementary Table S1**. Primers used in this study.

**Acknowledgments**

We thank Michael Hothorn (University of Geneva, Geneva, Switzerland) for discussions of the project, Yanhai Yin (Iowa State University, Ames, USA), Shuhua Yang (China Agricultural University, Beijing, China), Claudia Oecking (University of Tübingen, Tübingen, Germany), Han Jiang (Shandong Agricultural University, Tai'an, China), Shujing Wu (Shandong Agricultural

University, Tai'an, China), Xuelu Wang (Henan University, Kaifeng, China), and Steve Huber (University of Illinois, Urbana, USA) for providing the α-BES1 antibody, the *pET28a-GRF6* construct, the amiRNA line *grf9,10,11*$^{RNAi}$, the split-ubiquitin system, the *pCB302-35S:GFP* constructs, the *p35S:BKI1-GFP*/Col-0 transgenic line, and α-p$S_{858}$ antibody, respectively, and Martine De Cock (VIB-Ghent University, Ghent, Belgium) for help in preparing the article. HOME for Researchers is acknowledged for linguistic assistance during the preparation of this manuscript.

**Funding**

The work was supported by National Natural Science Foundation of China (32370750 to D. Liu), Shandong Provincial Natural Science Foundation (ZR2023MC060 to D. Liu), and Shandong Agricultural University Start-up Fund (325/72398, 325/72401, 539/539383) to D. Luo and D. Liu, the Ghent University Special Research Fund Grant (BOF15/24J/048 to E.R.), and the Research Foundation-Flanders (project G008416N to E.R.).

**Data availability**

All the materials used in this study is available upon request to the corresponding author.

*Conflict of interest statement*. None declared.

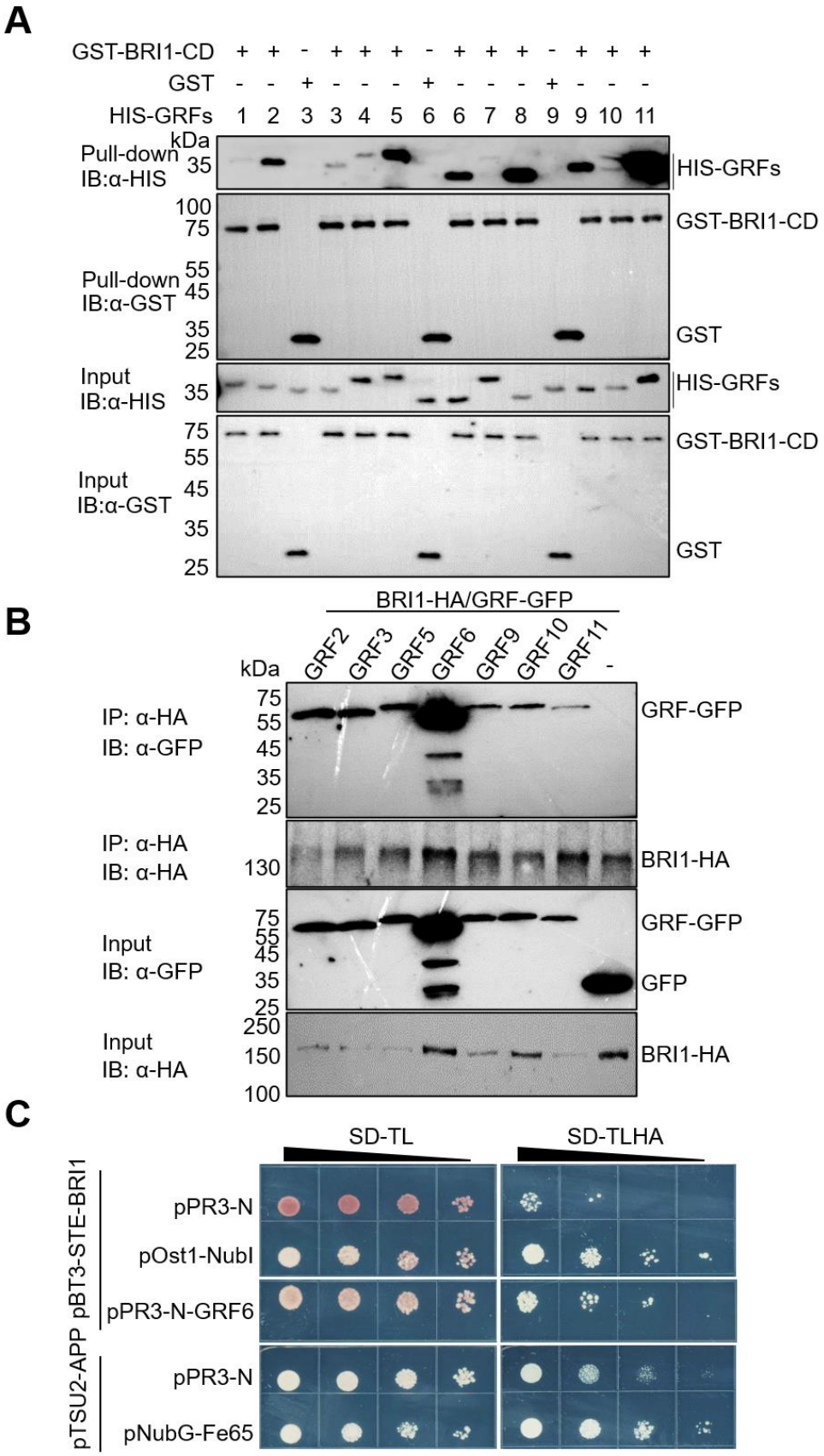
A
GST-BRI1-CD + + - + + + - + + + - + + +
GST - - + - - - + - - - + - - -
HIS-GRFs 1 2 3 3 4 5 6 6 7 8 9 9 10 11
kDa
Pull-down IB:α-HIS
35
HIS-GRFs
100
75
GST-BRI1-CD
Pull-down IB:α-GST
55
45
35
25
GST
Input IB:α-HIS
35
HIS-GRFs
75
55
45
35
25
GST-BRI1-CD
Input IB:α-GST
GST
B
BRI1-HA/GRF-GFP
kDa
GRF2
GRF3
GRF5
GRF6
GRF9
GRF10
GRF11
-
IP: α-HA IB: α-GFP
75
55
45
35
25
GRF-GFP
IP: α-HA IB: α-HA
130
BRI1-HA
Input IB: α-GFP
75
55
45
35
25
GRF-GFP
GFP
Input IB: α-HA
250
150
100
BRI1-HA
C
SD-TL
SD-TLHA
pBT3-STE-BRI1
pPR3-N
pOst1-NubI
pPR3-N-GRF6
pTSU2-APP
pPR3-N
pNubG-Fe65

**Figure 1.** 14-3-3s interact directly with BRI1. **A**) GRF1 to GRF11 interact with BRI1 *in vitro*. HIS-fused GRFs were incubated with glutathione beads alone or coupled with GST or GST-fused BRI1-cytoplasmic domain (CD; GST-BRI1-CD). The beads were collected, washed, and immunoblotted (IB) with α-GST and α-HIS antibodies. Protein inputs were determined with α-GST and α-HIS antibodies. **B**) Association between BRI1 and GRFs *in planta*. *N. benthamiana* leaves co-expressing GFP-tagged GRFs or free GFP together with HA-tagged BRI1 were collected 48 h post-agroinfiltration. Co-immunoprecipitation (co-IP) assays using α-HA beads were done with proteins isolated from these samples. Proteins were subjected to immunoblot (IB) assay using α-HA and α-GFP antibodies. **C**) Mating based split-ubiquitin assay of the interaction between BRI1 and GRF6. *pTSU2-APP/pNubG-Fe65*, systemic positive control; *pTSU2-APP/pPR3N*, systemic negative control; *pBT3-STE-BRI1/pPR3N*, self-activation control; *pBT3-STE-BRI1/pOst1-NubI*, positive control for BRI1; and *pBT3-STE-BRI1/pPR3N-GRF6*, combination of interest. SD-TL, control medium (SD/-Trp-Leu); SD-TLHA, selective medium (SD/-Trp-Leu-His-Ade). Ten-fold serial dilutions of the saturated cultures were spotted onto plates. The blots in A) and B) were performed twice, and similar results were obtained.

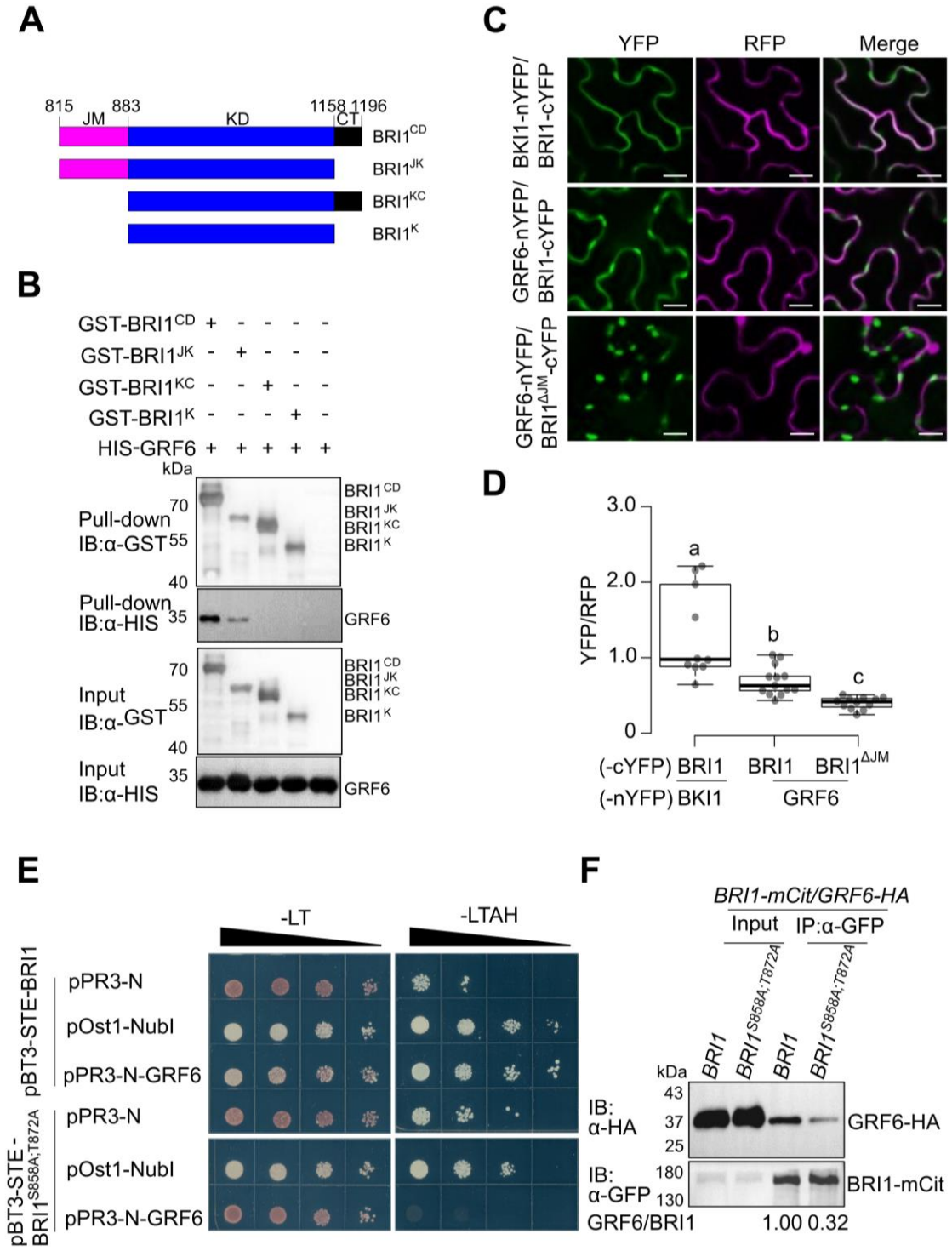


**Figure 2**. S858 and T872 in the JM domain of BRI1 are required for the 14-3-3-binding to BRI1. **A**) Diagrams showing different truncated forms of BRI1-CD. **B**) GRF6 interaction with BRI1 *in vitro* in the JM domain. HIS-fused GRF6 was incubated with glutathione beads alone or coupled with the GST-fused truncated BRI1-cytoplasmic domain, as shown in (**A**). The beads were

collected, washed, and immunoblotted with α-GST and α-HIS antibodies. Protein inputs were also determined using α-GST and α-HIS IBs. **C** and **D**) rBiFC analysis of BRI1 and BRI1$^{\Delta JM}$ (BRI1 with JM deletion) with GRF6 in *N. benthamiana* leaf epidermal cells. The combination BKI1-nYFP/BRI1-cYFP was used as positive control. Quantification of YFP against RFP fluorescence signal ratios for different combinations is shown in (**D**). $n$=10, $n$, cell number. Scale bar, 10 µm. Different letters indicate significant differences ($P < 0.05$, one-way ANOVA followed by Tukey's test). **E**) Mating based split-ubiquitin assay of the interactions between BRI1 or BRI1$^{S858A;T872A}$ and GRF6. *pBT3-STE-BRI1/pPR3N* and *pBT3-STE-BRI1$^{S858A;T872A}$/pPR3N* are self-activation controls for BRI1 and BRI1$^{S858A;T872A}$, *pBT3-STE-BRI1/pOst1-NubI* and *pBT3-STE-BRI1$^{S858A;T872A}$/pOst1-NubI* are positive controls for BRI1 and BRI1$^{S858A;T872A}$, and *pBT3-STE-BRI1/pPR3N-GRF6* and *pBT3-STE-BRI1$^{S858A;T872A}$/pPR3N-GRF6* show the interactions between BRI1 and GRF6 or between BRI1$^{S858A;T872A}$ and GRF6. Ten-fold serial dilutions of the saturated cultures were spotted onto plates. **F**) Impaired association of BRI1 with GRF6 in Arabidopsis by the S858A and T872A mutations in BRI1. Rosetta leaves of 3-week-old Arabidopsis transgenic lines co-expressing mCitrine (mCit)-tagged BRI1 or BRI1$^{S858A;T872A}$ and HA-tagged GRF6 were harvested for co-immunoprecipitation (co-IP) using α-GFP-coated beads. Proteins were subjected to immunoblot (IB) assay using α-HA and α-GFP antibodies. The signal ratios of GRF6 versus BRI1 are shown below the blots. The blots in B) and F) were performed twice, and similar results were obtained.

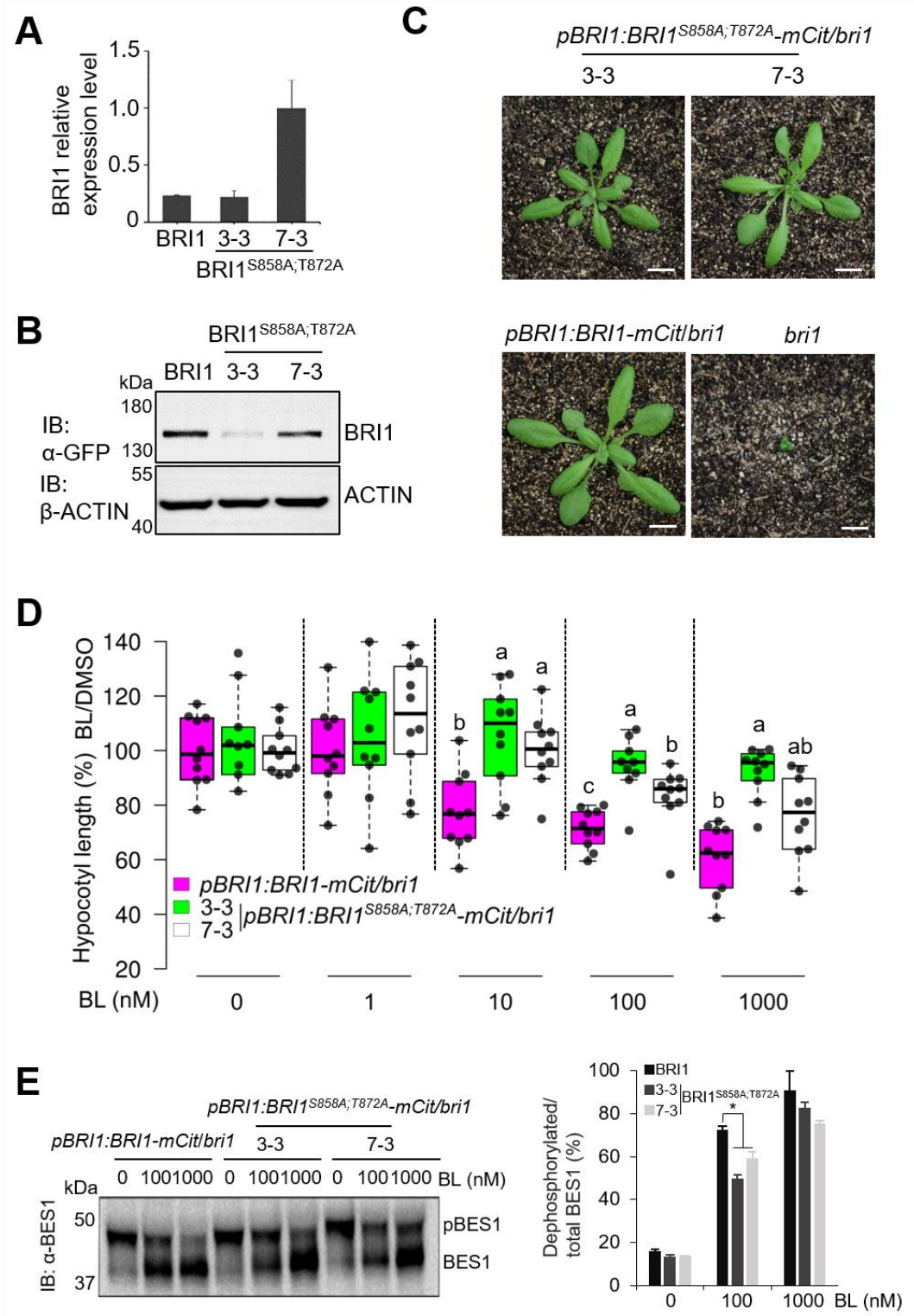


**Figure 3.** BRI1 carrying S858A and T872A mutations only partially complemented the *bri1* null mutant. **A** and **B**) Molecular characterization of *Arabidopsis* transgenic lines harboring S858A and

T872A mutations in BRI1. **A**) Real-time quantitative reverse transcription-PCR analysis of *BRI1*. Total RNA was isolated from 5-day-old seedlings. *ACTIN2* expression was used as an internal control. Error bars indicate standard deviation (SD); $n$ = three biological replicates. **B**) Immunoblot (IB) analysis of BRI1 expression. Total proteins were isolated from 5-day-old seedlings of the transgenic lines and detected using an α-GFP antibody (top). Protein inputs were equilibrated by immunoblot (IB) assay with the β-ACTIN antibody (bottom). **C**) Growth phenotypes of soil-grown 4-week-old homozygous plants. Scale bar, 1 cm. **D**) Sensitivity to brassinolide (BL) of transgenic lines shown by hypocotyl length. Hypocotyl length (normalized to the DMSO control) of 5-day-old seedlings grown in the dark and in the presence of increasing BL concentrations. For each transgenic line at each concentration, at least nine seedlings were measured. Different letters indicate a significant difference with others ($P < 0.05$, one-way ANOVA followed by Tukey's test). **E**) Five-day-old seedlings treated with DMSO, 100 nM BL, or 1000 nM BL for 1 h subjected to IB assay using α-BES1 antibody. dpBES1, dephosphorylated BES1. Percentage of dpBES1 relative to the total BES1 were measured ($n$ = 3 biological replicates).

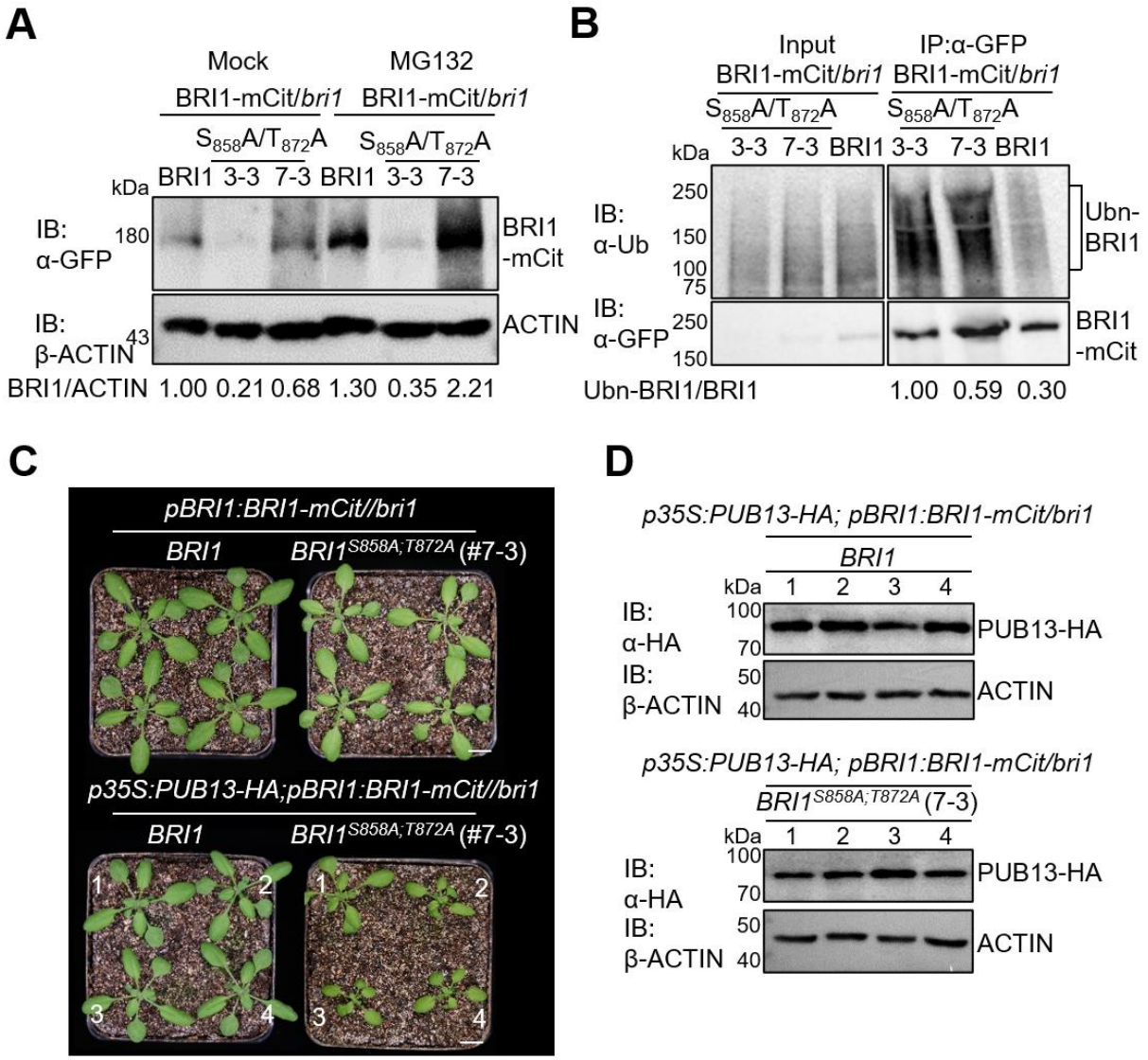


**Figure 4.** S858A and T872A mutations reduced the protein abundance of BRI1. **A**) BRI1$^{S858A;T872A}$ abundance depends on the 26S proteasome. Six-day-old seedlings of the indicated lines were treated with 50 µM MG132 or an equal volume of DMSO for 5 h before harvesting for total protein isolation. BRI1 protein amount was determined by IB with the α-BRI1 antibody (top), and protein inputs were equilibrated by immunoblot (IB) assay with the β-ACTIN antibody (bottom). The signal ratios of BRI1 versus ACTIN are shown below the blots. **B**) Increased BRI1 ubiquitination in BRI1$^{S858A;T872A}$. Immunoprecipitation (IP) was performed using α-GFP-coated magnetic beads on solubilized microsomal fraction proteins isolated from 6-day-old seedlings of the indicated transgenic lines after treatment with MG-132 (50 µM) for 5 h and subjected to IB assay with α-ubiquitin (top) and α-GFP (bottom). The ratios between ubiquitinated BRI1 and total BRI1 ($Ub_n$-

BRI1/BRI1-mCit) were calculated and are shown below the blots. **C**) Growth phenotypes of the soil-grown 23-day-old *p35S:PUB13-HA;pBRI1:BRI1-mCit/bri1* and *p35S:PUB13-HA;pBRI1:BRI1*$^{S858A;T872A}$*-mCit/bri1* (#7-3) plants, together with the indicated control lines. Scale bar, 1 cm. **D**) IB analysis of PUB13-HA expression. Total proteins isolated from the plants in (**C**) were detected using an α-HA antibody (top). Protein inputs were equilibrated by immunoblot (IB) assay with the β-ACTIN antibody (bottom).

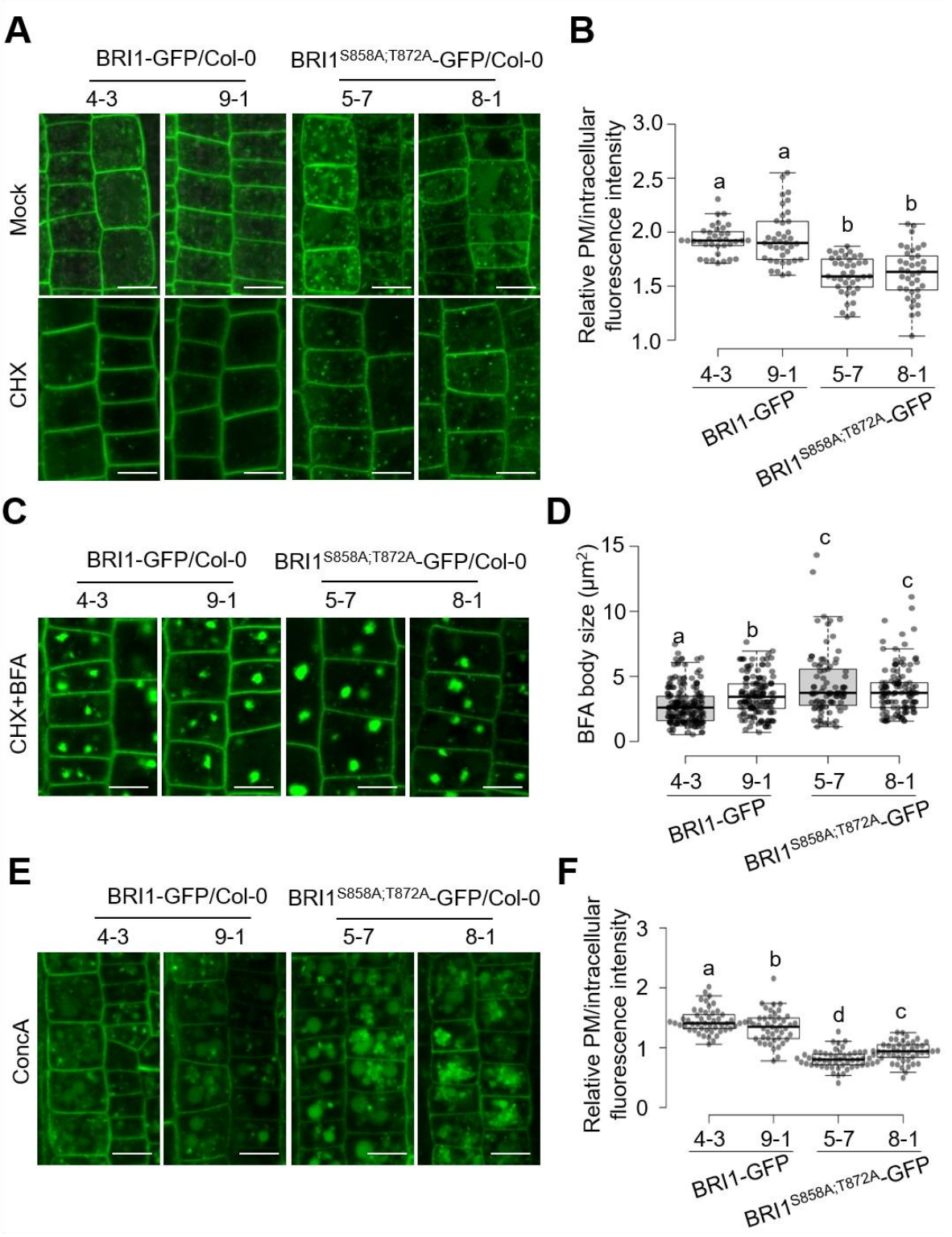


**Figure 5.** S858A and T872A mutations in BRI1 decreased the plasma membrane (PM) pool of BRI1and increased its internalization, and targeting to the vacuole. **A** and **C**) Images of epidermal

cells from root meristems of 5-day-old transgenic Arabidopsis seedlings expressing WT or S858A;T872A-mutated BRI1 tagged with GFP pretreated with cycloheximide (CHX) (50 µM) for 1.5 h (**A**) or pretreated with CHX (50 µM) for 1 h, followed by a combined treatment with CHX (50 µM) and BFA (50 µM) for 30 min (**C**). **B** and **D**) Measurements of the relative PM versus intracellular BRI1-GFP fluorescence intensity and BFA body size derived from the images displayed in (**A**) and (**C**). At least 36 cells from five seedlings were measured for each transgenic line. **E**) Sensitivity to ConcA of BRI1-GFP/Col-0 and $BRI1^{S858A;T872A}$-GFP/Col-0 plants. Five-day-old seedlings of the indicated lines were exposed to ConcA (1 µM) for 2 h. **F**) Measurements of the relative PM versus intracellular BRI1-GFP fluorescence intensity from the images displayed in (**E**). Similar confocal detection settings were used to compare different lines under different chemical treatments. Scale bar, 10 µm in (**A**), (**C**), and (**E**). Different letters in (**B**), (**D**), and (**F**) indicate significant differences ($P < 0.05$, one-way ANOVA followed by Tukey's test).

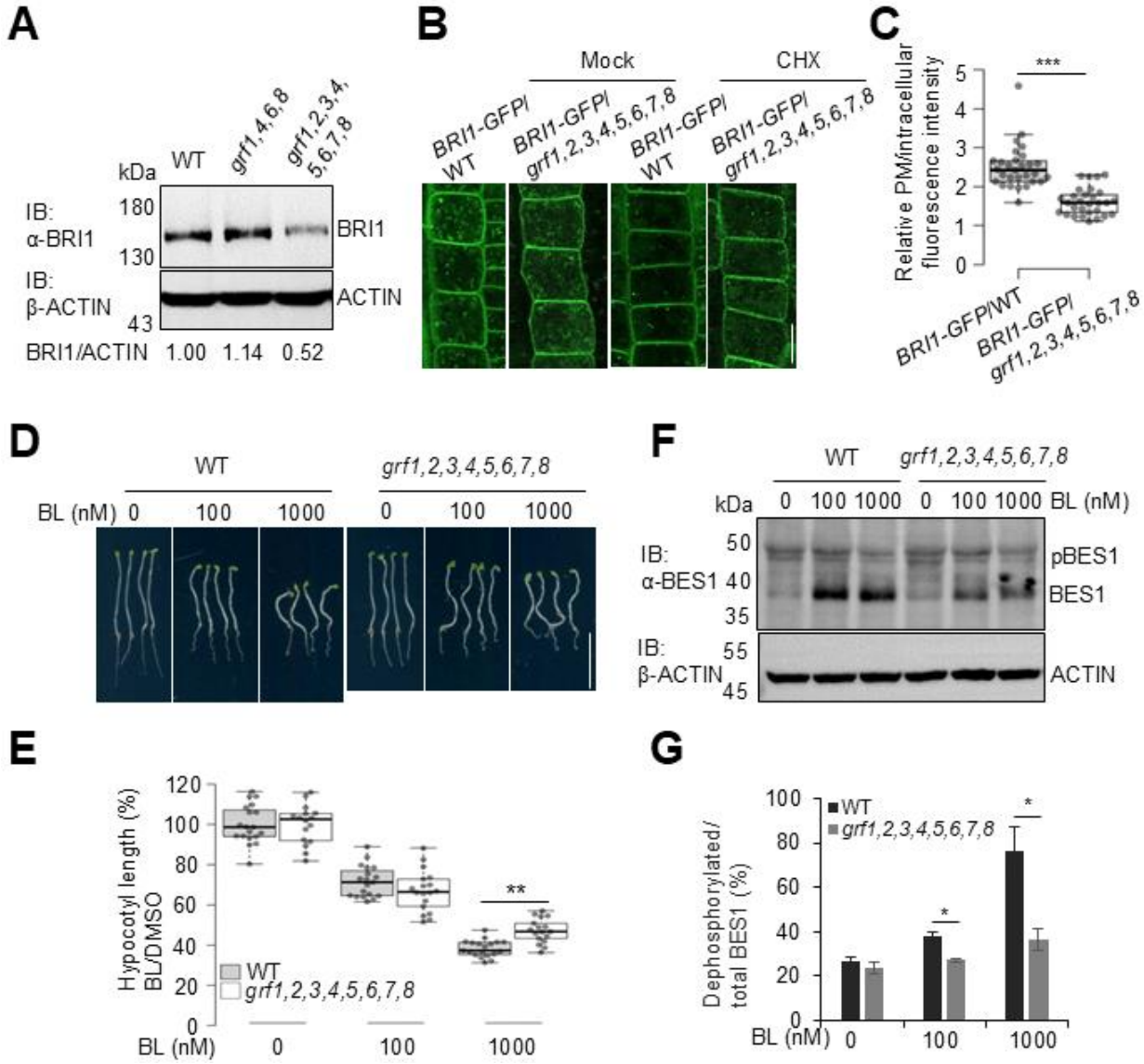


**Figure 6.** Knocking out *GRF2*, *GRF3*, *GRF5*, and *GRF7* in *grf1,4,6,8* resulted in BRI1 degradation, increased BRI1 endocytosis, and hyposensitivity of plants to BRs. **A**) Reduced BRI1 stability in *grf1,2,3,4,5,6,7,8* compared to the controls. Total proteins were isolated from 6-day-old seedlings of the indicated lines. The amount of BRI1 protein was determined by immunoblot (IB) assay with the α-BRI1 antibody (top), and ACTIN was used as loading control by IB assay with the β-ACTIN antibody (bottom). The signal ratios of BRI1 versus ACTIN are shown below the blots. **B** and **C**) Enhanced BRI1 endocytosis in *grf1,2,3,4,5,6,7,8* than in WT background. **B**) Images of epidermal cells from root meristems of 6-day-old T1 screened Arabidopsis seedlings expressing BRI1 tagged with GFP pretreated with cycloheximide (CHX) (50 µM) for 1.5 h. **C**) Measurements of the relative PM versus intracellular BRI1-GFP fluorescence intensity derived from the images

displayed in the right panel in (**B**). At least 30 cells from four seedlings were measured for each background. **D** and **E**) Growth phenotype of 5-day-old seedlings of the dark-grown indicated lines treated with BL at 0, 100, and 1000 nM. Hypocotyl lengths of the seedlings shown in (**D**) were measured and shown in (**E**). For each transgenic line, at least 16 seedlings were measured. *$P < 0.05$; **$P < 0.01$, Student *t*-test. Scale bar in (**D**), 1 cm. **F** and **G**) BES1 dephosphorylation assay. Five-day-old seedlings treated with BL at 0, 100, and 1000 nM for 1 h were subjected to IB assay using the α-BES1 antibody. The β-ACTIN IB was used for loading control. Percentages of dephosphorylated BES1 relative to the total BES1 were shown in bar charts in (**G**) (n = 2 biological replicates).

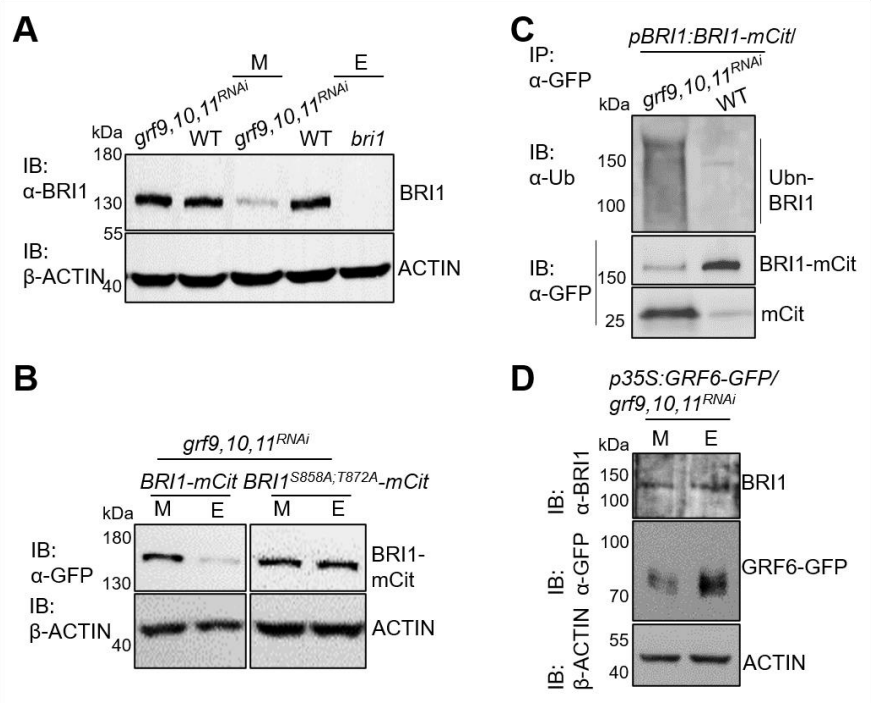


**Figure 7.** Inducible knock down of the epsilon subgroup isoforms *GRF9*, *GRF10*, and *GRF11* (*grf9,10,11*$^{RNAi}$) resulted in BRI1 degradation. **A** and **B**) Immunoblotting (IB) analysis of BRI1 and BRI1-mCitrine (mCit) abundance. Total protein was isolated from 7-day-old seedlings of the indicated lines grown in a medium containing 0.1% (v/v) ethanol (E) or mock (M). The total protein amount isolated from homozygous *bri1* was used as negative control to demonstrate the specificity of the α-BRI1 antibody. BRI1 and BRI1-mCit were detected using α-BRI1 and α-GFP antibodies, respectively (top). ACTIN was used as loading control by IB with the β-ACTIN antibody (bottom). **C**) Increased BRI1 ubiquitination in *grf9,10,11*$^{RNAi}$. Immunoprecipitation (IP) was performed using α-GFP-coated beads on solubilized microsomal fraction proteins isolated from 6-day-old seedlings of the indicated transgenic lines grown in 0.1% (v/v) ethanol-containing medium after further treatment with MG-132 (50 µM) for 5 h. Protein were subjected to IB assays with α-ubiquitin (top) and α-GFP (bottom). **D**) Stabilized BRI1 in ethanol-treated *grf9,10,11*$^{RNAi}$ by *GRF6* overexpression. T1 seeds of *p35S:GRF6-GFP/grf9,10,11*$^{RNAi}$ were screened on medium containing 0.1% (v/v) ethanol (E) or mock (M) with the presence of Kanamycin. The total protein isolated from resistant seedlings were blotted with α-BRI1, α-GFP, and β-ACTIN antibodies to detect the levels of BRI1, GRF6-GFP and protein input, respectively.

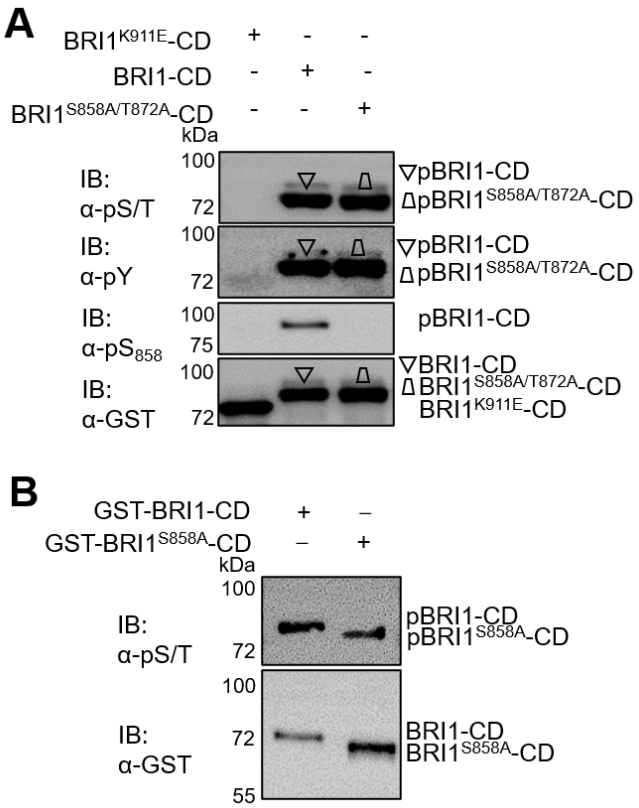


**Supplementary Figure S1**. Effect of S858A and T872A mutations on BRI1 kinase activity *in vitro*. **A** and **B**) Effects of S858A;T872A double or S858A single residue substitutions in BRI1-CD on their autophosphorylation status. Equal amounts of recombinant N-terminally GST-tagged cytoplasmic domain (CD) of wild-type BRI1, kinase-dead $BRI1^{K911E}$, $BRI1^{S858A}$ and $BRI1^{S858A;T872A}$ BRI1 mutants were used *in vitro* kinase reaction, followed by immunoblotting (IB) with modification-specific antibodies (α-pS/T, α-pY, and α-$pS_{858}$). pBRI1-CD and $pBRI1^{S858A;T872A}$-CD indicate the specifically phosphorylated proteins. Different shapes indicate GST-BRI1-CD or GST-$BRI1^{S858A;T872A}$-CD, or phosphorylated ones, respectively as indicated. Protein loading is shown by IB assay with an α-GST antibody.

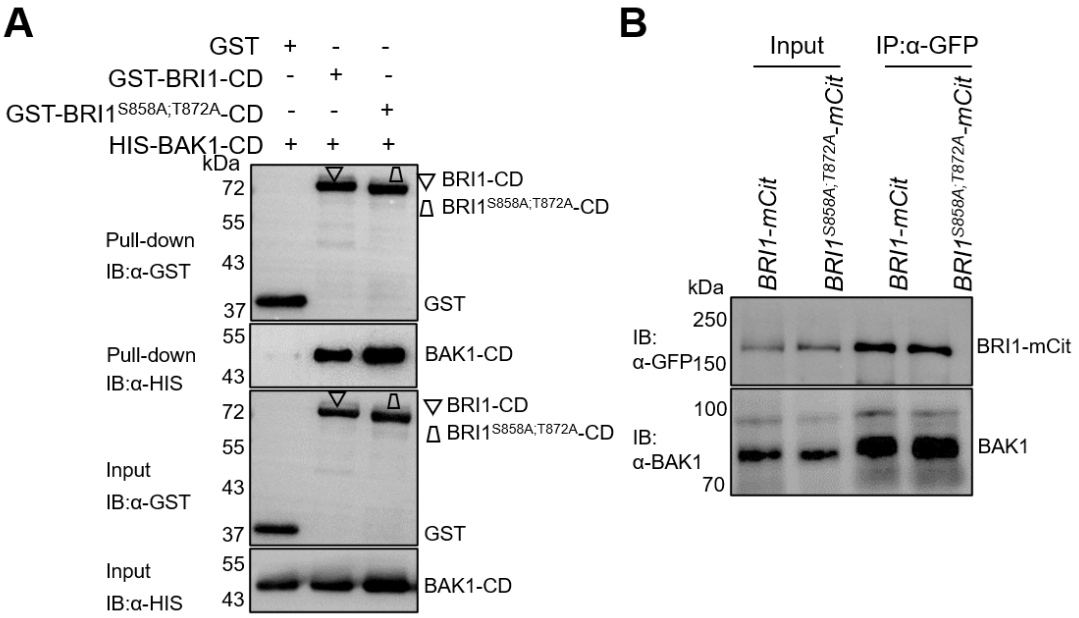


**Supplementary Figure S2.** BRI1 association with BAK1 was not affected by the S858A and T872A mutations in BRI1. **A**) BAK1 associations with wild-type BRI1 and BRI1$^{S858A;T872A}$ mutant determined by *in vitro* GST pull-down. HIS-fused BAK1 cytoplasmic domain (BAK1-CD) was incubated with free GST, GST-fused BRI1-CD, or BRI1$^{S858A;T872A}$-CD. The beads were collected and washed, and the pull-down fractions were followed by IBs with α-GST and α-HIS. Protein inputs were determined by immunoblotting (IB) with α-GST and α-HIS. **B**) BAK1 associations with wild-type BRI1 and BRI1$^{S858A;T872A}$ mutant in Arabidopsis. Eight-day-old Arabidopsis transgenic plants expressing mCitrine (mCit)-tagged BRI1 or BRI1BRI1$^{S858A;T872A}$ were first treated with 2 μM, brassinazole (BRZ), and for 3 days, followed by a treatment with 1 μM brassinolide (BL) for 90 min, and co-immunoprecipitation (co-IP) assays using α-GFP-coated beads were performed with proteins isolated from these samples. The proteins were subjected to immunoblotting (IB) using α-BAK1 and α-GFP antibodies.

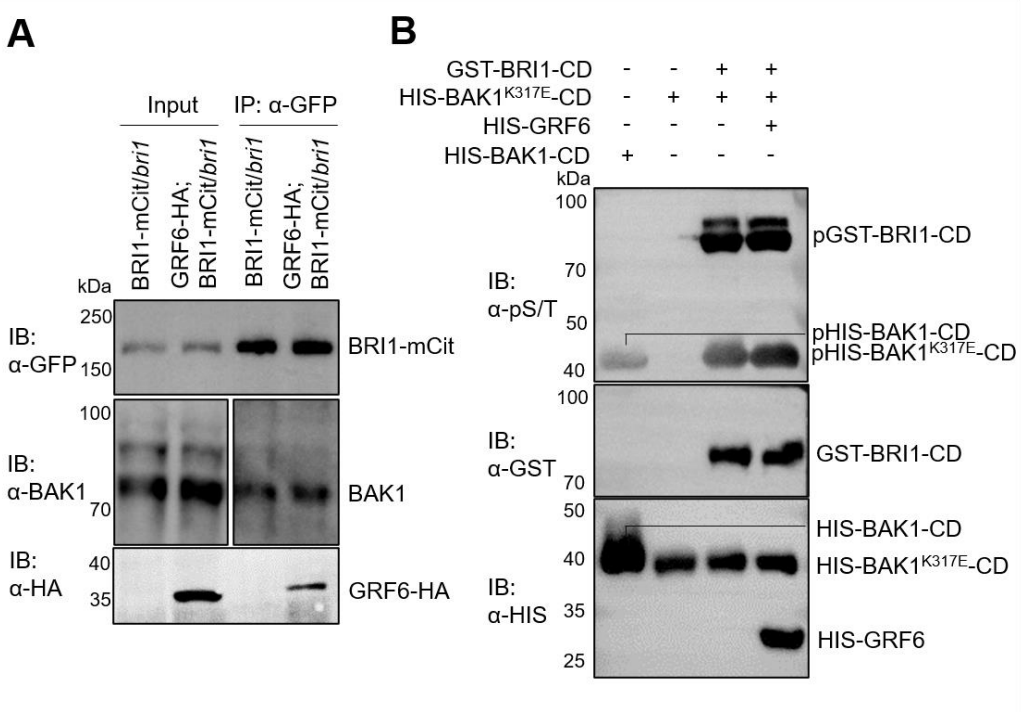


**Supplementary Figure S3.** BRI1 association with BAK1 and BRI1 kinase activity were unaffected by the presence of GRF6. **A**) The association between BRI1 and BAK1 in Arabidopsis was unaffected by the GRF6. Eight-day-old Arabidopsis transgenic plants expressing BRI1-mCitrine (mCit) alone or together with GRF6-HA were first treated with 2 µM BRZ for 3 days followed by 1 µM BL for 90 min, and subjected to co-immunoprecipitation (co-IP) using α-GFP-coated beads. The proteins were detected by immunoblotting (IB) with α-GFP, α-BAK1 and α-HA antibodies. **B**) Effect of GRF6 binding on BRI1 kinase activity. Recombinant HIS-BAK1$^{K317E}$-CD, HIS-GRF6, and GST-BRI1-CD proteins were incubated alone or in combination, as indicated. BRI1 or BAK1 phosphorylation was detected by IB with α-pS/T, and protein loading was determined by IB using α-GST and α-HIS antibodies.

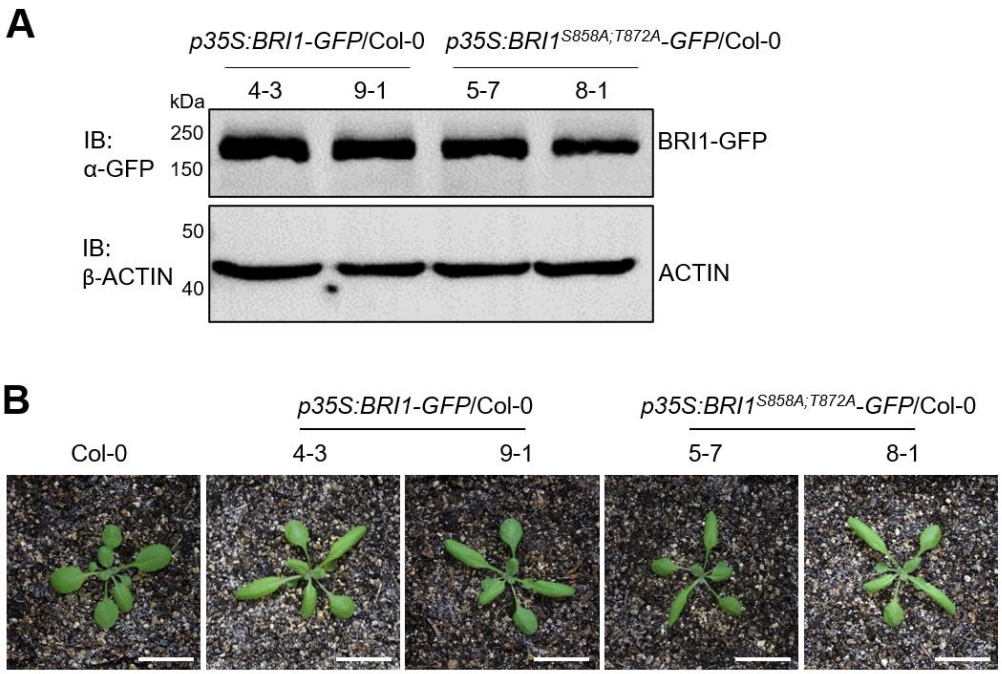


**Supplementary Figure S4.** Characterization of *p35S:BRI1-GFP*/Col-0 and *p35S:BRI1*$^{S858A;T872A}$-*GFP*/Col-0 transgenic plants. **A**) IB analysis of BRI1 expression. Total proteins were isolated from 5-day-old seedlings of the transgenic lines and detected using an α-GFP antibody (top). ACTIN was used as loading control by immunoblot (IB) assay with the β-ACTIN antibody (bottom). **B**) Growth phenotypes of soil-grown 26-day-old transgenic lines. Scale bar, 1 cm.

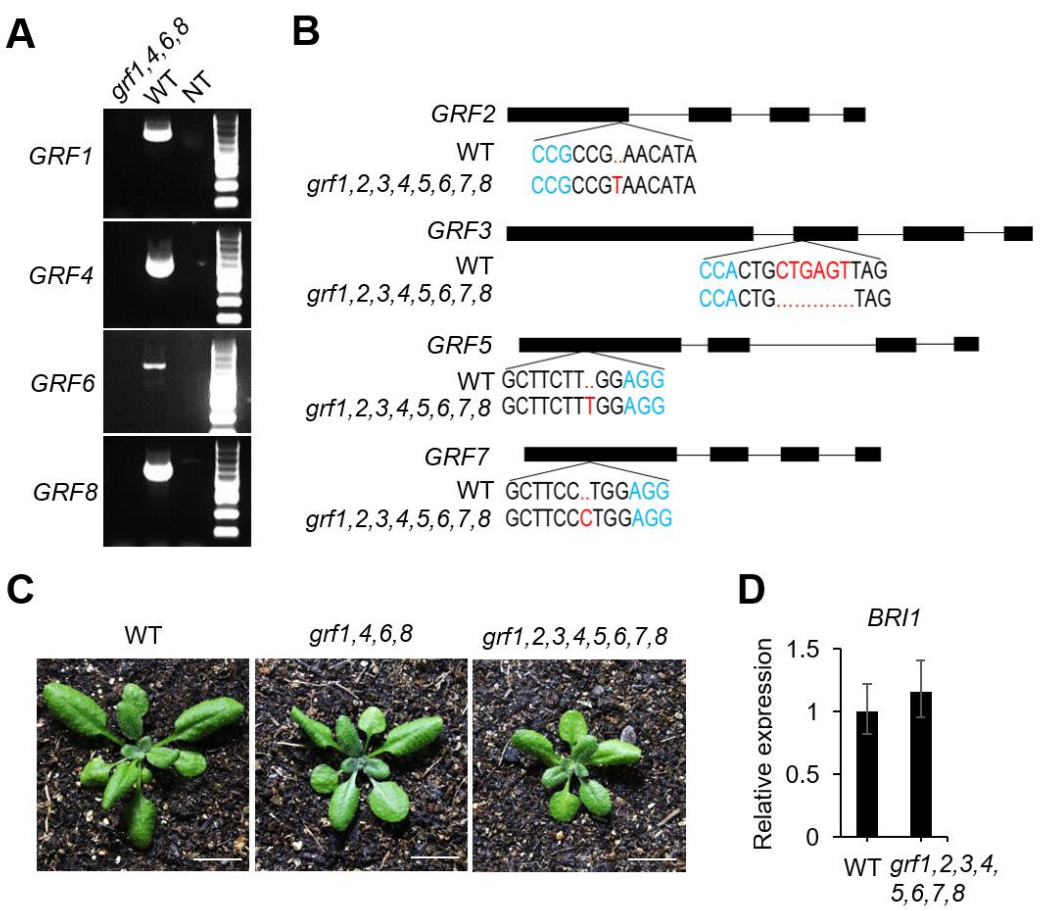


**Supplementary Figure S5.** Molecular characterization of the quadruple *grf1,4,6,8* mutant and octuple *grf1,2,3,4,5,6,7,8* mutant. **A**) Genotyping of quadruple *grf1,4,6,8* mutant. Genomic DNA isolated from *grf1,4,6,8* mutant and wild-type plants and the negative control (NT) were used for PCR analysis with gene-specific primers. **B**) Generation of *CR-2,3,5,7* quadruple mutants in *klpc* background using CRISPR/Cas9. The gene structures and resulting mutations in *GRF2*, *GRF3*, *GRF5*, and *GRF7* are illustrated. **C**) Growth phenotypes of soil-grown indicated lines at 22 °C, 56% relative humidity, and 16-h light/8-h dark for 26 days. Scale bar = 1 cm. **D**) qRT-PCR analyse of *BRI1* (*n* =3, *n*, biological replicates). Total RNA was isolated from 7-day-old seedlings grown in a medium. *ACTIN2* expression was used as an internal control. Error bars indicate standard deviation (SD). n = three independent experiments.

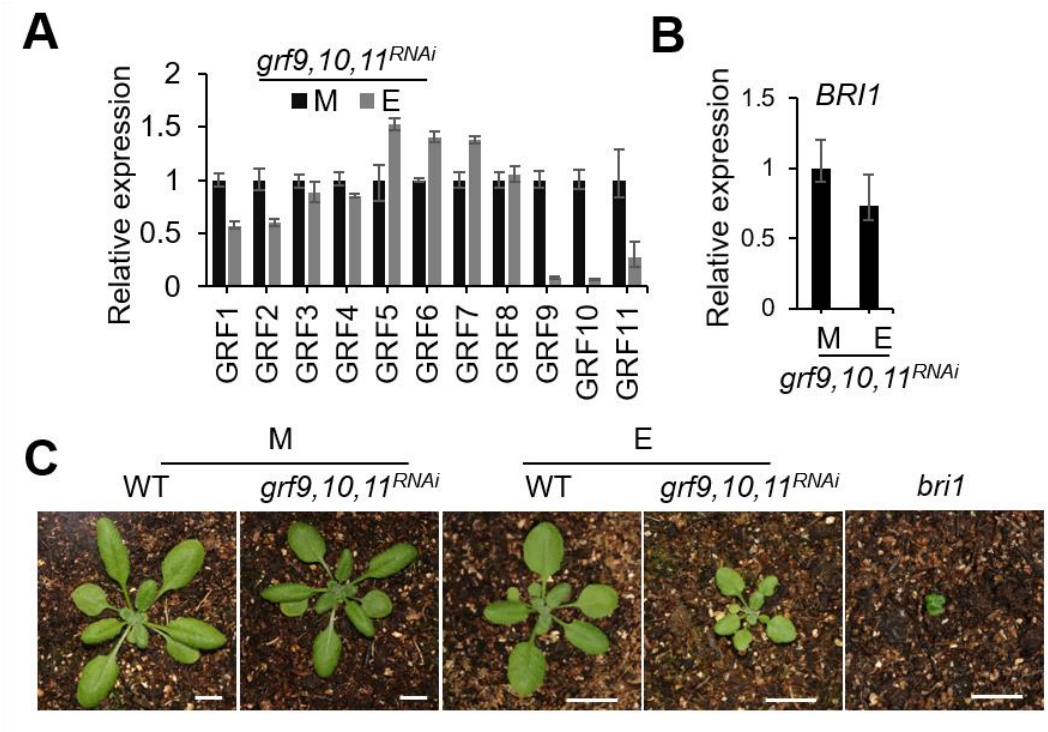


**Supplementary Figure S6**. Molecular characterization of the ethanol-inducible amiRNA line, *grf9,10,11*$^{RNAi}$. **A** and **B**) qRT-PCR analyses of *GRF1-11* and *BRI1* (*n* =3, *n*, biological replicates). Total RNA was isolated from 5-day-old seedlings grown in a medium with or without 0.1% (v/v) ethanol. *ACTIN2* expression was used as an internal control. Error bars indicate standard deviation (SD). n = three independent experiments. **C**) Growth phenotypes of soil-grown 22-day-old plants. The seeds were sown directly into the soil. Plants were sprayed with $H_2O$ or 1% (v/v) ethanol-containing water from day 7 every other day (two spays per plant) until day 21. Plants were photographed on day 22. Scale bars, 1 cm.

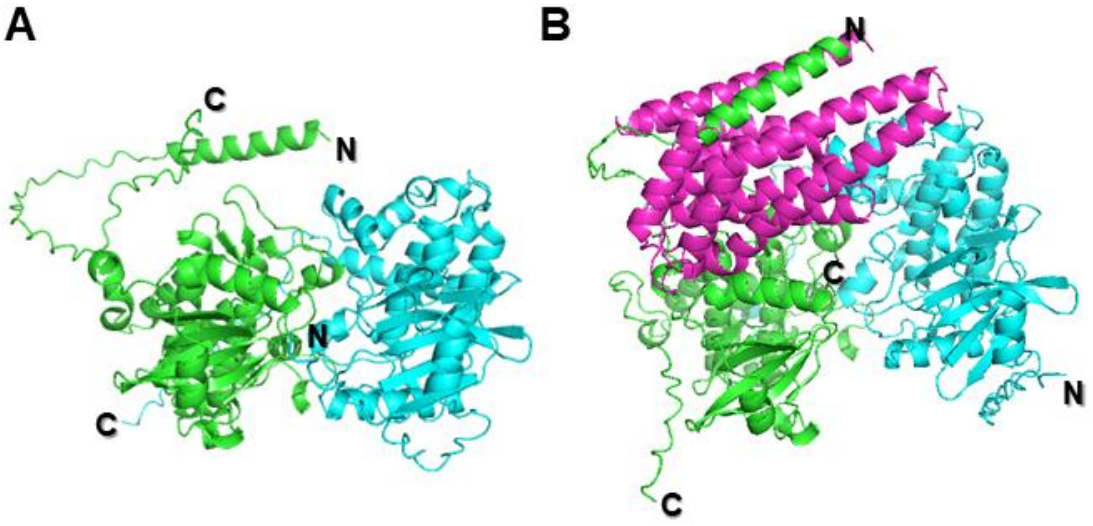


**Supplementary Figure S7**. Three-dimensional structure of BRI1-CD/BAK1-CD dimmer and BRI1-CD/BAK1-CD/GRF6 trimer predited by AlphaFold. BRI1-CD, BAK1-CD, together without or with GRF6 protein sequences were entried at AlphaFold Server (AlphaFold Server) to generate the BRI1-CD/BAK1-CD dimmer (**A**) or BRI1-CD/BAK1-CD/GRF6 trimer (**B**) structures, repectively. The secondary strucures shown in green, blue, and magenta represent BRI1-CD, BAK1-CD, and GRF6, respectlvely. The N' and C'-ternimals of BRI1-CD and BAK1-CD were labeled with N and C.

## References


**Aitken, A.** Post-translational modification of 14-3-3 isoforms and regulation of cellular function. Semin. Cell Biol. 2011:**22**(7):673-680. https://doi.org/10.1016/j.semcdb.2011.08.003

**Alsterfjord, M, Sehnke, PC, Arkell, A, Larsson, H, Svennelid, F, Rosenquist, M, Ferl, RJ, Sommarin, M, Larsson, C.** Plasma membrane $H^+$-ATPase and 14-3-3 isoforms of *Arabidopsis* leaves: evidence for isoform specificity in the 14-3-3/$H^+$-ATPase interaction. Plant Cell Physiol. 2004:**45**(9):1202-1210. https://doi.org/10.1093/pcp/pch136

**Caño-Delgado, A, Yin, Y, Yu, C, Vafeados, D, Mora-García, S, Cheng, J-C, Nam, KH, Li, J, Chory, J.** BRL1 and BRL3 are novel brassinosteroid receptors that function in vascular differentiation in *Arabidopsis*. Development. 2004:**131**(21):5341-5351. https://doi.org/10.1242/dev.01403

**Chae, WB, Park, Y-J, Lee, KS, Nou, I-S, Oh, M-H.** Plant receptor kinases bind and phosphorylate 14-3-3 proteins. Genes Genom. 2016:**38**(11):1111-1119. https://doi.org/10.1007/s13258-016-0468-5

**Chang, I-F, Curran, A, Woolsey, R, Quilici, D, Cushman, JC, Mittler, R, Harmon, A, Harper, JF.** Proteomic profiling of tandem affinity purified 14-3-3 protein complexes in *Arabidopsis thaliana*. Proteomics. 2009:**9**(11):2967-2985. https://doi.org/10.1002/pmic.200800445

**Claus, LAN, Liu, D, Hohmann, U, Vukašinović, N, Pleskot, R, Liu, J, Schiffner, A, Jaillais, Y, Wu, G, Wolf, S, Van Damme, D, Hothorn, M, Russinova, E.** BRASSINOSTEROID INSENSITIVE1 internalization can occur independent of ligand binding. Plant Physiol. 2023:**192**(1):65-76. https://doi.org/10.1093/plphys/kiad005

**Concordet, J-P, Haeussler, M.** CRISPOR: intuitive guide selection for CRISPR/Cas9 genome editing experiments and screens. Nucleic Acids Res. 2018:**46**(W1):W242-W245. https://doi.org/10.1093/nar/gky354

**Darling, DL, Yingling, J, Wynshaw-Boris, A.** Role of 14–3–3 proteins in eukaryotic signaling and development. Curr Top Dev Biol. 2005:**68**:281-315. https://doi.org/10.1016/S0070-2153(05)68010-6

**Decaestecker, W, Buono, RA, Pfeiffer, ML, Vangheluwe, N, Jourquin, J, Karimi, M, Van Isterdael, G, Beeckman, T, Nowack, MK, Jacobs, TB.** CRISPR-TSKO: a technique for

efficient mutagenesis in specific cell types, tissues, or organs in Arabidopsis. Plant Cell. 2019:**31**(12):2868-2887. https://doi.org/10.1105/tpc.19.00454

**Denison, FC, Paul, A-L, Zupanska, AK, Ferl, RJ.** 14-3-3 proteins in plant physiology. Semin Cell Dev Biol. 2011:**22**(7):720-727. https://doi.org/10.1016/j.semcdb.2011.08.006

**Di Rubbo, S, Irani, NG, Kim, SY, Xu, Z-Y, Gadeyne, A, Dejonghe, W, Vanhoutte, I, Persiau, G, Eeckhout, D, Simon, S, Song, K, Kleine-Vehn, J, Friml, J, De Jaeger, G, Van Damme, D, Hwang, I, Russinova, E.** The clathrin adaptor complex AP-2 mediates endocytosis of BRASSINOSTEROID INSENSITIVE1 in *Arabidopsis*. Plant Cell. 2013:**25**(8):2986-2997. https://doi.org/10.1105/tpc.113.114058

**Friedrichsen, DM, Joazeiro, CAP, Li, J, Hunter, T, Chory, J.** Brassinosteroid-insensitive-1 is a ubiquitously expressed leucine-rich repeat receptor serine/threonine kinase. Plant Physiol. 2000:**123**(4):1247-1256. https://doi.org/10.1104/pp.123.4.1247

**Fuglsang, AT, Borch, J, Bych, K, Jahn, TP, Roepstorff, P, Palmgren, MG.** The binding site for regulatory 14-3-3 protein in plant plasma membrane $H^+$-ATPase: involvement of a region promoting phosphorylation-independent interaction in addition to the phosphorylation-dependent c-terminal end. J Biol Chem. 2003:**278**(43):42266-42272. https://doi.org/10.1074/jbc.M306707200

**Gadeyne, A, Sánchez-Rodríguez, C, Vanneste, S, Di Rubbo, S, Zauber, H, Vanneste, K, Van Leene, J, De Winne, N, Eeckhout, D, Persiau, G, Van De Slijke, E, Cannoot, B, Vercruysse, L, Mayers, Jonathan R, Adamowski, M, Kania, U, Ehrlich, M, Schweighofer, A, Ketelaar, T, Maere, S, Bednarek, SY, Friml, J, Gevaert, K, Witters, E, Russinova, E, Persson, S, De Jaeger, G, Van Damme, D.** The TPLATE adaptor complex drives clathrin-mediated endocytosis in plants. Cell. 2014:**156**(4):691-704. https://doi.org/10.1016/j.cell.2014.01.039

**Gampala, SS, Kim, T-W, He, J-X, Tang, W, Deng, Z, Bai, M-Y, Guan, S, Lalonde, S, Sun, Y, Gendron, JM, Chen, H, Shibagaki, N, Ferl, RJ, Ehrhardt, D, Chong, K, Burlingame, AL, Wang, Z-Y.** An essential role for 14-3-3 proteins in brassinosteroid signal transduction in *Arabidopsis*. Dev Cell. 2007:**13**(2):177-189. https://doi.org/10.1016/j.devcel.2007.06.009

**Geldner, N, Friml, J, Stierhof, Y-D, Jürgens, G, Palme, K.** Auxin transport inhibitors block PIN1 cycling and vesicle trafficking. Nature. 2001:**413**(6854):425-428. https://doi.org/10.1038/35096571

**Geldner, N, Hyman, DL, Wang, X, Schumacher, K, Chory, J.** Endosomal signaling of plant steroid receptor kinase BRI1. Genes Dev. 2007:**21**(13):1598-1602. https://doi.org/10.1101/gad.1561307

**Gietz, RD, Schiestl, RH.** High-efficiency yeast transformation using the LiAc/SS carrier DNA/PEG method. Nat Protoc. 2007:**2**(1):31-34. https://doi.org/10.1038/nprot.2007.13

**Grefen, C, Blatt, MR.** A 2in1 cloning system enables ratiometric bimolecular fluorescence complementation (rBiFC). Biotechniques. 2012:**53**(5):311-314. https://doi.org/10.2144/000113941

**He, Z, Wang, Z-Y, Li, J, Zhu, Q, Lamb, C, Ronald, P, Chory, J.** Perception of brassinosteroids by the extracellular domain of the receptor kinase BRI1. Science. 2000:**288**(5475):2360-2363. https://doi.org/10.1126/science.288.5475.2360

**Huang, Y, Wang, W, Yu, H, Peng, J, Hu, Z, Chen, L.** The role of 14-3-3 proteins in plant growth and response to abiotic stress. Plant Cell Rep. 2021:**1**:1-20. https://doi.org/10.1007/s00299-021-02803-4

**Irani, NG, Di Rubbo, S, Mylle, E, Van den Begin, J, Schneider-Pizoń, J, Hniliková, J, Šíša, M, Buyst, D, Vilarrasa-Blasi, J, Szatmári, A-M, Van Damme, D, Mishev, K, Codreanu, M-C, Kohout, L, Strnad, M, Caño-Delgado, AI, Friml, J, Madder, A, Russinova, E.** Fluorescent castasterone reveals BRI1 signaling from the plasma membrane. Nat Chem Biol. 2012:**8**(6):583-589. https://doi.org/10.1038/nchembio.958

**Jaillais, Y, Hothorn, M, Belkhadir, Y, Dabi, T, Nimchuk, ZL, Meyerowitz, EM, Chory, J.** Tyrosine phosphorylation controls brassinosteroid receptor activation by triggering membrane release of its kinase inhibitor. Genes Dev. 2011:**25**(3):232-237. https://doi.org/10.1101/gad.2001911

**Jiang, J, Wang, T, Wu, Z, Wang, J, Zhang, C, Wang, H, Wang, Z-X, Wang, X.** The intrinsically disordered protein BKI1 is essential for inhibiting BRI1 signaling in plants. Mol Plant. 2015:**8**(11):1675-1678. https://doi.org/10.1016/j.molp.2015.07.012

**Johnson, C, Crowther, S, Stafford, Margaret J, Campbell, David G, Toth, R, MacKintosh, C.** Bioinformatic and experimental survey of 14-3-3-binding sites. Biochem J. 2010:**427**(1):69-78. https://doi.org/10.1042/BJ20091834

**Jumper, J, Evans, R, Pritzel, A, Green, T, Figurnov, M, Ronneberger, O, et al**. Highly accurate protein structure prediction with AlphaFold. Nature 2021:**596**:583-589. doi: 10.1038/s41586-021-03819-2

**Keicher, J, Jaspert, N, Weckermann, K, Möller, C, Throm, C, Kintzi, A, Oecking, C.** *Arabidopsis* 14-3-3 epsilon members contribute to polarity of PIN auxin carrier and auxin transport-related development. eLife. 2017:**6**:e24336. https://doi.org/10.7554/eLife.24336

**Kim, T-W, Park, CH, Hsu, C-C, Kim, Y-W, Ko, Y-W, Zhang, Z, Zhu, J-Y, Hsiao, Y-C, Branon, T, Kaasik, K, Saldivar, E, Li, K, Pasha, A, Provart, NJ, Burlingame, AL, Xu, S-L, Ting, AY, Wang, Z-Y.** Mapping the signaling network of BIN2 kinase using TurboID-mediated biotin labeling and phosphoproteomics. Plant Cell. 2023:**35**(3):975-993. https://doi.org/10.1093/plcell/koad013

**Kinoshita, T, Caño-Delgado, A, Seto, H, Hiranuma, S, Fujioka, S, Yoshida, S, Chory, J.** Binding of brassinosteroids to the extracellular domain of plant receptor kinase BRI1. Nature. 2005:**433**(7022):167-171. https://doi.org/10.1038/nature03227

**Lee, JH, Kwak, G, Lim, YP, Oh, M-H.** 14-3-3 proteins contribute to leaf and root development via brassinosteroid insensitive 1 in *Arabidopsis thaliana*. Genes Genom. 2020:**42**(3):347-354. https://doi.org/10.1007/s13258-019-00909-4

**Li, J, Wen, J, Lease, KA, Doke, JT, Tax, FE, Walker, JC.** BAK1, an *Arabidopsis* LRR receptor-like protein kinase, interacts with BRI1 and modulates brassinosteroid signaling. Cell. 2002:**110**(2):213–222. https://doi.org/10.1016/S0092-8674(02)00812-7

**Lin, W, Lu, D, Gao, X, Jiang, S, Ma, X, Wang, Z, Mengiste, T, He, P, Shan, L.** Inverse modulation of plant immune and brassinosteroid signaling pathways by the receptor-like cytoplasmic kinase BIK1. Proc Natl Acad Sci USA. 2013:**110**(29):12114-12119. https://doi.org/10.1073/pnas.1302154110

**Liu, Z, Jia, Y, Ding, Y, Shi, Y, Li, Z, Guo, Y, Gong, Z, Yang, S.** Plasma membrane CRPK1-mediated phosphorylation of 14-3-3 proteins induces their nuclear import to fine-tune CBF signaling during cold response. Mol Cell. 2017:**66**(1):117-128. https://doi.org/10.1016/j.molcel.2017.02.016

**Liu, D, Kumar, R, Claus, LAN, Johnson, AJ, Siao, W, Vanhoutte, I, Wang, P, Bender, KW, Yperman, K, Martins, S, Zhao, X, Vert, G, Van Damme, D, Friml, J, Russinova, E.**

Endocytosis of BRASSINOSTEROID INSENSITIVE1 is partly driven by a canonical Tyr-based motif. Plant Cell. 2020:**32**(11):3598-3612. https://doi.org/10.1105/tpc.20.00384

**Luo, Y, Scholl, S, Doering, A, Zhang, Y, Irani, NG, Di, S, Neumetzler, L, Krishnamoorthy, P, Van Houtte, I, Mylle, E, Bischoff, V, Vernhettes, S, Winne, J, Friml, J. Stierhof, Y, Schumacher, K, Persson, S, Russinova, E.** V-ATPase-Activity in the TGN/EE is required for exocytosis and recycling in Arabidopsis. Nat Plants. 2016:1:15094. https://doi.org/10.1038/nplants.2015.94

**Luo, Y, Takagi, J, Claus, LAN., Zhang, C, Yasuda, S, Hasegawa, Y, Yamaguchi, J, Shan, L, Russinova, E, Sato, T.** Deubiquitinating enzymes UBP12 and UBP13 stabilize the brassinosteroid receptor BRI1. EMBO Rep. 2022:**23**:e53354. https://doi.org/10.15252/embr.202153354

**Martins, S, Dohmann, EMN, Cayrel, A, Johnson, A, Fischer, W, Pojer, F, Satiat-Jeunemaître, B, Jaillais, Y, Chory, J, Geldner, N, Vert, G.** Internalization and vacuolar targeting of the brassinosteroid hormone receptor BRI1 are regulated by ubiquitination. Nat Commun. 2015:**6**:6151. https://doi.org/10.1038/ncomms7151

**Nam, KH, Li, J.** BRI1/BAK1, a receptor kinase pair mediating brassinosteroid signaling. Cell. 2002:**110**(2):203–212. https://doi.org/10.1016/S0092-8674(02)00814-0

**Nolan, TM, Vukašinović, N, Liu, D, Russinova, E, Yin, Y.** Brassinosteroids: multidimensional regulators of plant growth, development, and stress responses. Plant Cell. 2020:**32**(2):295-318. https://doi.org/10.1105/tpc.19.00335

**Obergfell, E, Hohmann, U, Moretti, A, Chen, H, Hothorn, M.** Mechanistic insights into the function of 14-3-3 proteins as negative regulators of brassinosteroid signaling in *Arabidopsis*. Plant Cell Physiol. 2024:**in press**:pcae056. https://doi.org/10.1093/pcp/pcae056

**Oh, M-H, Wang, X, Clouse, SD, Huber, SC.** Deactivation of the *Arabidopsis* BRASSINOSTEROID INSENSITIVE 1 (BRI1) receptor kinase by autophosphorylation within the glycine-rich loop. Proc Natl Acad Sci USA. 2012:**109**(1):327-332. https://doi.org/10.1073/pnas.1108321109

**Pallucca, R, Visconti, S, Camoni, L, Cesareni, G, Melino, S, Panni, S, Torreri, P, Aducci, P.** Specificity of ε and non-ε isoforms of *Arabidopsis* 14-3-3 proteins towards the $H^+$-ATPase and other targets. PLoS ONE. 2014:**9**(3):e90764. https://doi.org/10.1371/journal.pone.0090764

**Paul, A-L, Dension, FC, Schultz, ER, Zupanska, AK, Ferl, RJ.** 14-3-3 phosphoprotein interaction networks – does isoform diversity present functional interaction specification? Front Plant Sci. 2012:**3**:190. https://doi.org/10.3389/fpls.2012.00190

**Puntervoll, P, Linding, R, Gemünd, C, Chabanis-Davidson, S, Mattingsdal, M, Cameron, S, Martin, DM, Ausiello, G, Brannetti, B, Costantini, A, et al.** (2003). ELM server: a new resource for investigating short functional sites in modular eukaryotic proteins. Nucleic Acids Res. 2003:**31**(13):3625-3630. https://doi.org/10.1093/nar/gkg545

**Qi, H, Lei, X, Wang, Y, Yu, S, Liu, T, Zhou, S-K, Chen, J-Y, Chen, Q-F, Qiu, R-L, Jiang, L, Xiao, S.** 14-3-3 proteins contribute to autophagy by modulating SINAT-mediated degradation of ATG13. Plant Cell. 2022:**34**(12):4857-4876. https://doi.org/10.1093/plcell/koac273

**Reuter, L, Schmidt, T, Manishankar, P, Throm, C, Keicher, J, Bock, A, Droste-Borel, I, Oecking, C.** Light-triggered and phosphorylation-dependent 14-3-3 association with NON-PHOTOTROPIC HYPOCOTYL 3 is required for hypocotyl phototropism. Nat Commun. 2021:**12**(1):6128. https://doi.org/10.1038/s41467-021-26332-6

**Rienties, IM, Vink, J, Borst, JW, Russinova, E, de Vries, SC.** The *Arabidopsis* SERK1 protein interacts with the AAA-ATPase AtCDC48, the 14-3-3 protein GF14λ and the PP2C phosphatase KAPP. Planta. 2005:**221**(3):394-405. https://doi.org/10.1007/s00425-004-1447-7

**van Kleeff, PJM, Jaspert, N, Li, KW, Rauch, S, Oecking, C, de Boer, AH.** Higher order *Arabidopsis* 14-3-3 mutants show 14-3-3 involvement in primary root growth both under control and abiotic stress conditions. J Exp Bot. 2014:**65**(20):5877-5888. https://doi.org/10.1093/jxb/eru338

**Wang, X, Chory, J.** Brassinosteroids regulate dissociation of BKI1, a negative regulator of BRI1 signaling, from the plasma membrane. Science. 2006:**313**(5790):1118-1122. https://doi.org/10.1126/science.1127593

**Wang, Z-Y, Seto, H, Fujioka, S, Yoshida, S, Chory, J.** BRI1 is a critical component of a plasma-membrane receptor for plant steroids. Nature. 2001:**410**(6826):380–383. https://doi.org/10.1038/35066597

**Wang, B, Yang, H, Liu, Y-C, Jelinek, T, Zhang, L, Ruoslahti, E, Fu, H.** Isolation of high-affinity peptide antagonists of 14-3-3 proteins by phage display. Biochemistry. 1999:**38**(38):12499-12504. https://doi.org/10.1021/bi991353h

**Wang, X, Kota, U, He, K, Blackburn, K, Li, J, Goshe, MB, Huber, SC, Clouse, SD.** Sequential transphosphorylation of the BRI1/BAK1 receptor kinase complex impacts early events in brassinosteroid signaling. Dev Cell. 2008:**15**(2):220-235. https://doi.org/10.1016/j.devcel.2008.06.011

**Wang, X, Goshe, MB, Soderblom, EJ, Phinney, BS, Kuchar, JA, Li, J, Asami, T, Yoshida, S, Huber, SC, Clouse, SD.** Identification and functional analysis of in vivo phosphorylation sites of the Arabidopsis BRASSINOSTEROID-INSENSITIVE1 receptor kinase. Plant Cell. 2005:**17**(6):1685-1703. https://doi.org/10.1105/tpc.105.031393

**Wang, H, Yang, C, Zhang, C, Wang, N, Lu, D, Wang, J, Zhang, S, Wang, Z-X, Ma, H, Wang, X.** Dual role of BKI1 and 14-3-3 s in brassinosteroid signaling to link receptor with transcription factors. Dev Cell. 2011:**21**(5):825-834. https://doi.org/10.1016/j.devcel.2011.08.018

**Wang, L, Li, H, Lv, X, Chen, T, Li, R, Xue, Y, Jiang, J, Jin, B, Baluška, F, Šamaj, J, Wang, X, Lin, J.** Spatiotemporal dynamics of the BRI1 receptor and its regulation by membrane microdomains in living *Arabidopsis* cells. Mol Plant. 2015:**8**(9):1334-1349. https://doi.org/10.1016/j.molp.2015.04.005

**Wilson, RS, Swatek, KN, Thelen, JJ.** Regulation of the regulators: post-translational modifications, subcellular, and spatiotemporal distribution of plant 14-3-3 proteins. Front Plant Sci. 2016:**7**:611. https://doi.org/10.3389/fpls.2016.00611

**Wu, X.** Crosstalk of protein phosphorylation and lysine acetylation on 14-3-3 proteins and their applications in brassinosteroid signaling and photosynthesis. Doctoral thesis (University of Illinois at Urbana-Champaign). 2011. https://www.ideals.illinois.edu/items/25018

**Yang, Z, Wang, C, Xue, Y, Liu, X, Chen, S, Song, C, Yang, Y, Guo, Y.** Calcium-activated 14-3-3 proteins as a molecular switch in salt stress tolerance. Nat Commun. 2019:**10**(1):1199. https://doi.org/10.1038/s41467-019-09181-2

**Yin, Y, Wang, Z-Y, Mora-Garcia, S, Li, J, Yoshida, S, Asami, T, Chory, J.** BES1 accumulates in the nucleus in response to brassinosteroids to regulate gene expression and promote stem elongation. Cell. 2002:**109**(2):181–191. https://doi.org/10.1016/S0092-8674(02)00721-3

**Zhou, J, Liu, D, Wang, P, Ma, X, Lin, W, Chen, S, Mishev, K, Lu, D, Kumar, R, Vanhoutte, I, Meng, X, He, P, Russinova, E, Shan, L.** Regulation of *Arabidopsis* brassinosteroid receptor BRI1 endocytosis and degradation by plant U-box PUB12/PUB13-mediated ubiquitination. Proc Natl Acad Sci USA. 2018:**115**(8):E1906-E1915. https://doi.org/10.1073/pnas.1712251115